The Tribomechadynamics Research Challenge: Confronting blind predictions for the linear and nonlinear dynamics of a thin-walled jointed structure with measurement results

Malte Krack[a], Matthew R. W. Brake[d], Christoph Schwingshackl[b], Johann Gross[a], Patrick Hippold[a], Matias Lasen[b], Daniele Dini[b], Loic Salles[c], Matthew S. Allen[e], Drithi Shetty[d], Courtney A. Payne[e], Kai Willner[f], Michael Lengger[f], Moheimin Y. Khan[g], Jonel Ortiz[g], David A. Najera-Flores[h], Robert J. Kuether[g], Paul R. Miles[g], Chao Xu[i], Huiyi Yang[i], Hassan Jalali[j], Javad Taghipour[k], Hamed Haddad Khodaparast[k], Michael I. Friswell[k], Paolo Tiso[l], Ahmed Amr Morsy[l], Arati Bhattu[d], Svenja Hermann[m], Nidhal Jamia[k], H. Nevzat Özgüven[n], Florian Müller[a], Maren Scheel[a]

[a] *University of Stuttgart, Germany*
[b] *Imperial College London, UK*
[c] *University of Liege, Belgium*
[d] *Rice University Houston, USA*
[e] *Brigham Young University, USA*
[f] *Friedrich-Alexander-Universität Erlangen-Nürnberg, Germany*
[g] *Sandia National Laboratories, USA*
[h] *ATA Engineering Inc., USA*
[i] *Northwestern Polytechnical University, China*
[j] *Northumbria University, UK*
[k] *Swansea University, UK*
[l] *ETH Zurich, Switzerland*
[m] *TU Dortmund, Germany*
[n] *Middle East Technical University, Turkey*

Abstract

The present article summarizes the submissions to the Tribomechadynamics Research Challenge announced in 2021. The task was a blind prediction of the vibration behavior of a system comprising a thin plate clamped on two sides via bolted joints. Both geometric and frictional contact nonlinearities are expected to be relevant. Provided were the CAD models and technical drawings of all parts as well as assembly instructions. The main objective was to predict the frequency and damping ratio of the lowest-frequency mode as function of the amplitude. Many different prediction approaches were pursued, ranging from well-known methods to very recently developed ones. After the submission deadline, the system has been fabricated and tested. The aim of this article is to evaluate the current state of the art in modelling and vibration prediction, and to provide directions for future methodological advancements.

Keywords: friction damping, jointed structures, geometric nonlinearity, nonlinear dynamics, nonlinear modal analysis

1. Introduction

Jointed interfaces are ubiquitous in modern engineering as they allow structures to be composed of many sub-structures joined together via bolted (or other) connections. However, the physics of jointed interfaces is poorly understood, which results in inaccurate predictions of performance for novel, yet-to-be-fabricated structures. This presents a significant challenge for engineering as many industries are pushing for accelerated design cycles that result in fewer opportunities to build and test structures, so there are fewer opportunities to fit a nonlinear model to test data and use that to guide future design decisions. Since the establishment of a research community to study the mechanics of jointed structures collaboratively [1, 2, 3, 4], though, there has been significant progress in the modeling of jointed structures.

Much of the recent progress in modeling jointed structures has focused on using nonlinear, hysteretic elements [5] in a calibrated modeling framework - i.e., ones that update/optimize existing models to match experimental data. Calibrated modeling approaches are useful for interrogating how an existing structure will respond to novel excitations within a range bounded by the excitations used to generate the experimental data based on which the model was calibrated. There have been two main categories of calibrated modeling approaches – modal-based methods and location-based methods. Modal methods focus on matching the nonlinear components of each measured mode individually by introducing nonlinear elements to each considered mode of the structure [6, 7]. This is an efficient approach, but it does require the assumptions that modes do not interact, the nonlinearities are relatively weak (e.g., the stiffness of the structure does not change by more than a few percent), and the mode shapes do not change with excitation amplitude. Modal-based methods, though, are inadmissible for predicting the response of a novel structure as any calibrated modal-based model inherently convolutes the properties of the structure with the nonlinear characteristics of the joint (i.e., the properties of the joint cannot be disambiguated for use in a new structure). Location-based methods, conversely, spatially discretize the jointed interface and assume a nonlinear model based on the physical displacements of the interface [8, 9, 10, 11, 12, 13, 14]. This approach lends itself to decoupling the properties of the structure from the nonlinear characteristics of a joint, and can be used to provide an estimate of how a similar joint might perform in a novel structure [15]. Consequently, these methods are computationally expensive and require herculean efforts to match multiple modes [16, 17], rendering them ill-suited to studying large, complex structures (unlike the modal methods). As both methods are predicate on having experimental data to optimize the nonlinear elements against, neither approach is appropriate for making a prediction for a novel structure that has not been built or tested.

To surmount the challenge of predicting the response of a novel structure, tribomechadynamics [18, 19] (a modeling approach that simultaneously considers tribology, contact mechanics, and nonlinear/structural dynamics) was proposed as a means of understanding the physics of jointed interfaces and, ultimately, modeling jointed structures in a predictive manner. This has led to several experimental insights into the physics of jointed structures, including: the contact pressure internal to an interface fluctuates with time, both near the edges as well as under the frustrum of the bolts [20]; interfaces can exhibit receding contact in which the contact area changes dramatically over time [21, 22]; and the bolts are dynamically active participants in the jointed structure with time-varying strains [23, 11, 24]. Reconciling these observations with the modeling of jointed structures, along with more accurate contact models [25, 26], has led to accurate predictions of well-studied structures [26][1]. It remains to be seen, however, if a tribomechadynamic modeling approach will be successful for studying novel structures in which little is known a priori.

In 2021, the Tribomechadynamics Research Challenge (TRChallenge) was issued to the international community of researchers that study the mechanics of jointed structures. The goal of this challenge was to assess the potential of the state-of-the-art modeling approaches for predicting the dynamics of a novel structure with neither experimental data nor insights from prior design revisions. Specifically, the TRChallenge tasked researchers with predicting the linear frequencies and nonlinear characteristics (in terms of frequency and damping changes with response amplitude) of a thin panel bolted to a larger support structure. The design of the benchmark system was conducted in collaboration with researchers from industry to ensure that the design considerations reflected industrial best practices and that the challenges in modeling the benchmark system reflected the challenges faced by industrial researchers. The choice of a thin panel was due to their widespread use in aircraft, space, and wind turbine industries to achieve high strength-to-weight ratios; however, these slender structures are subjected to geometric and frictional nonlinearities because of large deformation and mechanical fasteners. Thus, the TRChallenge is multi-faceted in that there are interfacial nonlinearities, geometric nonlinearities, and multiple types of preload (from the initial shape being bent into a curved shape, and from the bolts used to assemble the structure). In fact, there is an interesting coupling between the two nonlinearities, as the contact behavior determines the axial stiffness, which has a crucial influence on the extent of the geometric nonlinearity associated to bending-stretching coupling, and the latter determines the tangential loading of the contact.

[1] Here, the behavior of a unique assembly was predicted based on highly detailed measurements of the interface topography down to the roughness length scale, which would not be available for a structure that has yet to be fabricated.

The format of this challenge was chosen based on the success of other similar challenges, such as the contact mechanics challenge [27] and the Sandia fracture challenges [28, 29, 30]. These two sets of challenges issued blind challenges (i.e., ones without experimental data for validation) to the contact mechanics community and fracture mechanics community, respectively, then assessed the different solutions submitted to the challenges against a truth solution. One advantage of this challenge format is that it allows for an un-biased assessment of the merits and deficiencies of different modeling approaches and, ultimately, is able to offer insights into future research directions to better meet such a challenge.
The remainder of this article is organized as follows: The TRChallenge is presented in Sect. 2. The different prediction approaches are summarized in Sect. 3. The experiment and the test procedure are described in Sect. 4. The results are shown and discussed in Sect. 5. Concluding remarks are given in Sect. 6.

2. Definition of the TRChallenge

The announcement of the challenge is available via `http://tmd.rice.edu/tribomechadynamics-research-challenge-2021/`. The CAD models, the technical drawings and the design documentation (including assembly instructions) are available in a data repository [31]. To make this article self-contained, the benchmark system and the tasks are summarized in the following.
The benchmark system of the challenge is depicted in Fig. 1. It consists of four main parts, a thin plate (*panel*), a support (monolithic piece comprising two pillars and a thick rear plate), and two blades. The panel has a thickness of 1.5 mm, its free part is 300 mm by 100 mm, and it is bolted between blades and pillars with six M6 bolts and washers, per side, spaced based on industry recommendations. The rear plate is to be bolted on the slip table of a large shaker. The panel's nominal initial geometry is flat. The contact surfaces with the pillars are flat, but deliberately misaligned by a nominal angle of 2.2° about the z-axis (1.1° inclination on each side), so that the panel is arched in the bolted configuration. The panel is made of stainless steel (AISI 301 material number 1.4310); support and blade are made of hardened steel (1.7147). Those materials are known for their high strength and high wear resistance, and they are commonly used in vibration test rigs. Special care was taken to achieve a well-defined and reproducible positioning of the panel between the blades and the support. To this end, a combination of centering holes and guide pins was used based on industrial best practices. Also, tightening order and torque (10.1 Nm for the M6, 40 Nm for the M10 bolts) were defined [31].
It is useful to explain some of the thoughts behind the particular architecture of the benchmark system. An important goal was to deviate considerably from the design of the previous benchmarks, in particular, the Brake-Reuss Beam [32] and the C-Beam [33]. This goal was set to avoid tempting teams into trying to

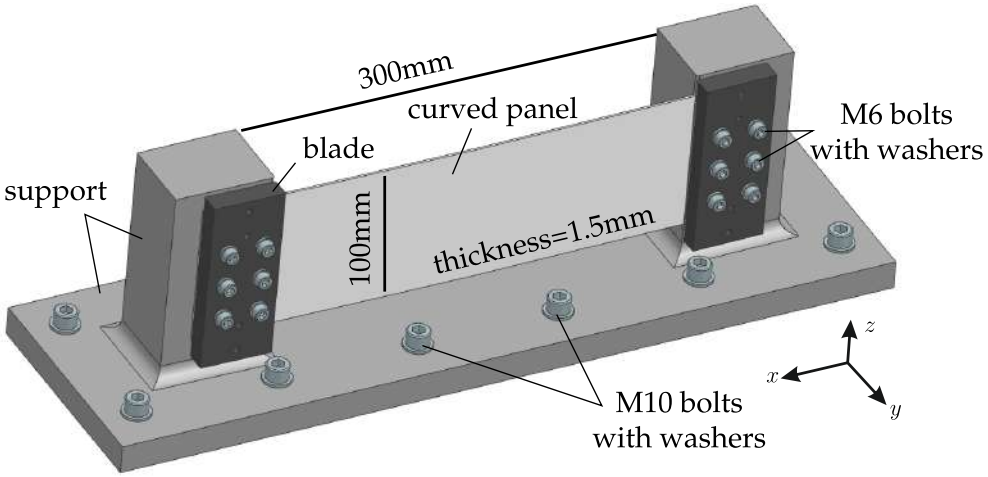

Figure 1: Benchmark system of the TRChallenge.

transfer empirical knowledge gained from those benchmarks, in order to enforce more predictive approaches. To achieve this, a novel feature was introduced that none of the existing benchmarks has: a doubly-clamped thin-walled component, which gives rise to geometrically nonlinear behavior due to bending-stretching coupling. The motivation behind introducing this particular novel feature was trigger more collaboration with the community focusing on geometrically nonlinear behavior. On the other hand, the benchmark system should have bolted joints to give rise to frictional contact nonlinearity, to ensure relevance to the joint mechanics community. This was achieved by the clamping of the panel, which introduced frictional contact between panel and support, and between panel and blades. It is well-known that nominally flat thin-walled structures (plates, beams) are highly sensitive to the clamping conditions and alignment tolerances, see e. g. [34, 35]. That is why an intentional misalignment of 2.2° was introduced by the support structure.
The participants were asked to predict the lowest natural frequency and the corresponding modal damping ratio as function of the vibration level at the panel center, ranging from zero to at least twice the thickness of the panel. Moreover, the natural frequencies of the five lowest-frequency elastic modes of the linearized system were requested (at asymptotically small vibration levels).

3. Prediction approaches

An overview of the research institutions that participated in the original challenge is given in Tab. 1. In the following, the abbreviation of the respective research institution will be used when referring to a specific prediction approach and the corresponding results. The TRChallenge was announced March 17th 2021. Six submissions were received by the deadline (September 30th 2021) specified in the announcement, or a few days later. Among these were the SU and the BYU-UW submissions of preliminary results, which were updated in February and October 2022, respectively. There are two more late submissions: USTUTT submitted in April 2022, and ETH in November 2022. On the one hand, including late submissions in this paper can be viewed as unfair towards the other contributing research institutions who managed to submit in time (and to those who decided not to participate due to the short deadline). On the other hand, the timely submissions largely relied on existing methodology, whereas the late submissions involved substantial method development, as detailed later. Since the intent of this work is to evaluate the state of the art in modelling and vibration prediction, we decided to include the late submissions. In any case, it is important to emphasize that the research groups involved in the predictions had no access to the experimental data acquired in August and September 2022 (to preseve the blind character of the prediction).
We regard the overall participation as a success, considering that no funding was centrally provided to support the activities of the participating groups. The reported results and chosen simplifications should be viewed in the light of limited resources and time frame, too. These limitations are not only inevitable but actually desired, because they are typical of the daily work within industry, much like the task to do a blind prediction itself, and are therefore consistent with the overall aim of the challenge.
The challenge was kept as open as possible and the participants were asked to use their best engineering

Table 1: Research groups that contributed so far to the TRChallenge. The submission date refers to the (possibly updated) version of the results shown in this paper.

Research institution	Abreviation	Submission date	References
Sandia National Laboratories, USA	SNL	10.2021	[36]
Friedrich-Alexander-Universität Erlangen-Nürnberg, Germany	FAU	09.2021	
Brigham Young University/University of Wisconsin-Madison, USA	BYU-UW	10.2022	[37, 38]
Northwestern Polytechnical University, China	NWPU	09.2021	
Imperial College London, UK	ICL	09.2021	[39]
University of Stuttgart, Germany	USTUTT	04.2022	[40]
ETH Zurich, Switzerland	ETH	11.2022	[41]
Swansea University, UK	SU	02.2022	

intuition to introduce reasonable simplifications in their modeling approach, select appropriate parameters and to use the preferred types of nonlinear analysis in order to obtain the amplitude-dependent modal properties. This led to a variety of prediction approaches, and of course also to some discrepancy in the results. It should be emphasized that even when the same prediction approach was used, some variability is to be expected simply because of distinct empirical input parameters that cannot yet be reliably predicted from first principles. In particular, friction coefficient, contact stiffness and bolt tension force selected by the different groups turned out to span a considerable range (cf. Tab. 5 in Subsect. 3.9), and the vibration behavior is known to depend sensitively on those parameters. It is useful to recall that the purpose of the challenge was to evaluate the state of the art in modeling and vibration prediction. The variability of the input parameters is completely in line with this goal. If, in contrast, the goal was to numerically validate a simplified modeling or analysis type, consistent parameters should be used. All selected prediction approaches have been numerically validated in separate studies (some references are provided in Tab. 1), and their limitations are largely well-known. The prediction approaches are described in the following. The results are summarized in Sect. 5 and confronted with the experimental reference.

Table 2: Dynamic analysis types and considered nonlinearities. QSMA: Quasi-static modal analysis. NMA: Nonlinear Modal Analysis. FRF: Frequency Response Analysis.

Research institution	dyn. analysis type	geometric nonlinearity	contact nonlinearity
BYU-UW	QSMA/NMA	yes	yes
FAU	QSMA	yes	yes
ETH	FRF	yes	yes
ICL	FRF	no	yes
NWPU	QSMA/Ring down	no	yes
SNL	Ring down	yes	yes
USTUTT	NMA	yes	yes
SU	FRF	no	yes

Before describing the individual approaches, it is useful to highlight some commonalities and differences. All eight submissions considered the frictional contact nonlinearity, while three neglect the geometric nonlinearity (Tab. 2). Those groups that consider the geometric nonlinearity started with a *preload simulation*, where the initially flat and unstressed panel was bolted to assume its arched configuration, and the pressure distribution in the contact areas was determined. One exception is the approach by FAU, where the panel was assumed as arched and aligned with the support structure in its initial, stress-free configuration. This preloaded configuration served as reference for linear modal analysis, and for the derivation of reduced component modes if a model order reduction approach was pursued. Finally, a certain type of dynamic analysis was carried out in order to identify the amplitude-dependent modal properties. Four types of dynamic analysis can be distinguished: *ring down simulation*, *quasi-static modal analysis* (QSMA), *frequency response analysis*, and *nonlinear modal analysis* (NMA). The titles of the following subsections specify the *type of dynamic analysis* used by the respective group, and whether the full finite element (FE) model or a reduced-order model (ROM) derived from this was used in that analysis. Also, it is specified if geometric nonlinearity was neglected. The presentation order is somewhat arbitrary. An overview, including a comparison of structural and contact modeling is given in Subsect. 3.9.

3.1. Ring down simulation of FE model (SNL)

The SNL team consisted of the co-authors M.Y. Khan, J. Ortiz, D.A. Najera, R.J. Kuether, and P.R. Miles. Their approach relied on a high-fidelity three-dimensional (3D) FE model, and all analysis steps, including the transient ring down, were carried out using state-of-the-art FE solvers. An important advantage of this approach is that practically arbitrary nonlinearities can be considered simultaneously, whereas ROM approaches are typically limited to a subset of nonlinearities and often do not allow to combine multiple nonlinearities within the same substructure.

Prior to meshing, simplifications were made to the CAD geometry to remove geometric features that were assumed negligible to the simulated quantities of interest. The bolts and through holes on the rear plate were removed, along with the hexagonal sockets on the cap screw heads and the guide pins used to mount the panel. Subsequently, a finite element mesh was generated using CUBIT [42] with 431,298 8-noded hexahedral (brick) elements. A selective deviatoric element formulation was used, which is fully integrated for the deviatoric stress response and under integrated for the hydrostatic pressure response [43]. To simplify the hexahedral meshing, rear plate and pillars were meshed separately and connected via tie constraints. A schematic of the mesh is provided in Fig. 2-left, where the inset shows a zoomed-in image of the interface between the blade, arched panel, and support (before applying the bolt preload). The entire back surface of the rear plate has fixed boundary conditions to approximate the assumed stiff mounting to the shaker during dynamic testing. It was assumed that material nonlinearity, such as plasticity, would not be present and thus the metals are modeled as homogenous, isotropic, and linear elastic. In fact, this assumption on the material behavior is common to all submissions and will thus not be explicitly stated in the following subsections.

Frictional contact was modeled at the following interfaces: bolt head to washer, washer to blade, blade to panel, and panel to support. During the nonlinear simulations, Coulomb friction was defined at all interfaces. The normal contact was modeled using an Augmented Lagrangian method with face-to-face contact enforcement at the interacting surfaces.

The preload simulation was conducted using the Sierra/Solid Mechanics (Sierra/SM) code [43]. The bolts were preloaded by applying an artificial strain of 0.0831 mm/mm to the block associated with the shank, i. e. the elements between bolt head and threaded region. The preload step was conducted using an explicit dynamic simulation with a piecewise linear ramp to first close the initial gap and deform the panel, then to apply the appropriate level of preload. The contact force under each bolt head was monitored to ensure a certain target value estimated from the specified tightening torque (10.1 Nm cf. Sect. 2). The simulation period was over 15 ms and velocity damping was applied to dissipate oscillations during the preload step. Once the oscillations were sufficiently settled and the force levels in the bolts were achieved, the simulation was deemed complete, and the results provide the predicted preloaded equilibrium state.

Following the bolt preload simulation, the model was linearized about the equilibrium state and a linear modal analysis was performed in the Sierra/Structural Dynamics (Sierra/SD) code. Subsequently, the nonlinear model was loaded by applying the distributed force $\alpha \boldsymbol{M}\boldsymbol{\phi}_1$ to all degrees of freedom in Sierra/SM, where $\boldsymbol{M}$ is the mass matrix and $\boldsymbol{\phi}_1$ is the lowest-frequency bending mode shape (obtained from the linear modal analysis). The scaling value α was specified so that the displacement at the panel center reaches 3 mm (two times the panel thickness). This force was applied using a cosine ramp. Subsequently, the force was instantaneously removed so that the structure rings down. All simulations in the Sierra/SM codes, i. e. bolt preload, applied modal force, and ring-down, rely on explicit time step integration [44]. A mass proportional damping model was applied, scaled so that the fundamental bending mode receives about 0.5 % damping. It should be noted that mass proportional damping is commonly selected in the case of explicit

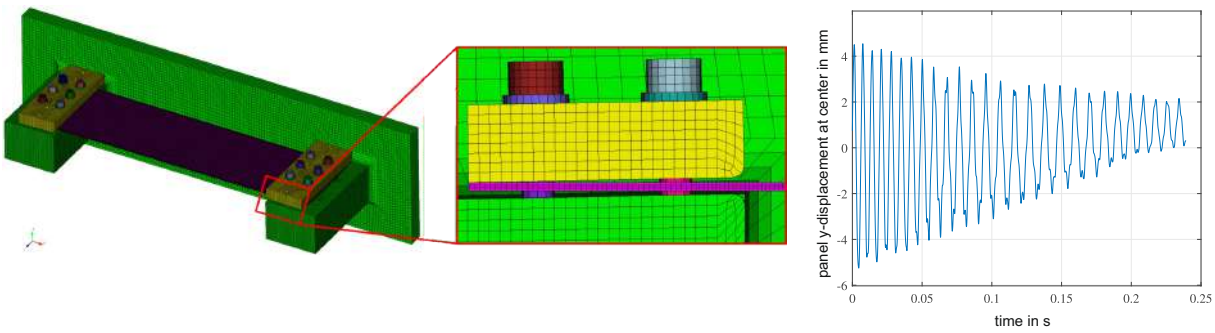

Figure 2: (left) SNL FE mesh, (right) ring-down response.

time step integration as it does not adversely affect the critical time step, as opposed to, e. g., stiffness-proportional damping. However, it was realized after the submission that it would be more appropriate to omit this damping and rely solely on the dissipation from the frictional elements. It was observed that this has relatively small influence on the amplitude-dependent frequency, but the identified damping is generally slightly lower when the mass-proportional damping is removed. The ring-down response shown in Fig. 2-right is post-processed using the short-time Fourier transform (STFT) to identify the amplitude-dependent frequency and damping [45]. Here, a Hanning window was applied to a short section of the signal, and the Fourier transform of the windowed signal provided an estimate of the instantaneous frequency and amplitude of the response at the time centered around the window. This process was repeated by shifting the window along the time axis, providing estimates of the frequency at discrete times of the ring down simulation. The instantaneous damping ratio was estimated from the exponential decay of the fundamental harmonic response from one discrete time to the next. The described STFT-based processing of the ring-down response has been shown to provide accurate modal frequency and damping results, and to outperform wavelet-based techniques when applied to jointed structures [46].
The main limitation of the described approach is the indirect identification of the amplitude-dependent modal parameters. The approach assumes that the force profile excites the structure in such a way that it predominately responds in the mode of interest during the ring down. It was observed, however, that the ring-down response (Fig. 2-right) has frequency content outside of the frequency of the target mode and its harmonics. This indicates modal coupling, which has the potential to contaminate the identified modal parameters, as discussed in [47] for a bolted structure. Another limitation is the long runtimes and computational resources needed to simulate high-fidelity solid mechanics models. A single query of the model, with the bolt preload, modal analysis, and modal force ring-down, requires approximately 50 hours of wall time to complete with 432 processors.

*3.2. QSMA of FE model (*FAU*)*

The FAU team consisted of the co-authors K. Willner and M. Lengger. Compared to the SNL model, the thick and stiff rear plate was neglected and instead the pillars were tied to the ground. Moreover, the bolts were not meshed with solid elements but instead with Timoshenko beam elements. The remaining parts were meshed with a total of ca. 10,000 tetrahedral elements with quadratic shape functions (C3D10).
The contact at the interfaces (panel-to-support and panel-to-blade) was modeled by a hard-contact in normal and a penalty formulation in the tangential direction with estimated values for the friction coefficient and an absolute elastic slip distance. Note that the stipulation of an elastic slip distance not only has a positive effect on the convergence behavior but also leads to a pressure-dependent tangential stiffness. Each bolt was preloaded uniformly and connected with Multi-Point Constraints to both the area occupied by the washer and the inner hole.
To determine the amplitude-dependent modal parameters, a Quasi-static Modal Analysis (QSMA) was used, as devised in [48], using a state-of-the-art FE tool (ABAQUS). As the panel is arched in its assembled configuration, the force–deflection behavior is asymmetric (Fig. 3-left), which violates a *Masing hypothesis*. Thus, complete hysteresis cycles cannot be simply constructed from a single initial modal loading curve. However, the natural frequency can still be computed from a composed modal force–deflection curve originating from the excitation of the preloaded system in two opposing load directions, as indicated in Fig. 3-left. This procedure leads to only moderate computational effort (ca. 7.5 hours wall time per curve using 4 cores with ABAQUS default setting on an Intel(R) Core(TM) i7-10700 CPU @ 2.90GHz (8CPUs), 32GB RAM), in contrast to simulating complete hysteresis cycles. The results obtained using both methods agree well, as shown in Fig. 3-right. Contrary to the natural frequency, a series of complete hysteresis cycles at several load amplitudes was required to estimate the amplitude-dependent modal damping ratio, which was associated with a tremendous computational burden. Here, the total strain energy E_p and the frictional dissipated energy ΔW were obtained directly from the ABAQUS output (ALLIE and ALLFD, respectively), to determine the damping ratio $D = \Delta W/(4\pi E_\mathrm{p}^\mathrm{max})$, see e. g. [49]. One of the inherent limitations to QSMA is that it does not account for any dynamic coupling between the modes nor allows one to predict any internal resonances.

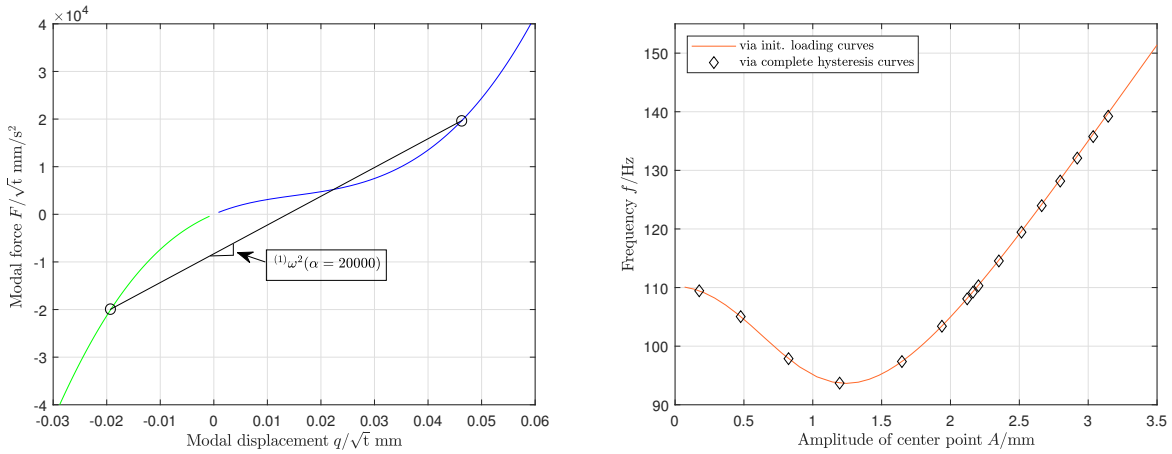

Figure 3: FAU approach to determine amplitude-dependent natural frequencies from a single composed initial loading curve (left) and comparison against results from a quasi-static sinusoidal excitation over six complete cycles (right). Note that mass-normalized deflection shapes have unit one over square-root of mass, so that the modal displacement has unit square-root mass times length, and the modal force has unit force divided by square-root of mass. Tons (t) and millimeters (mm) were used as mass and length unit, respectively.

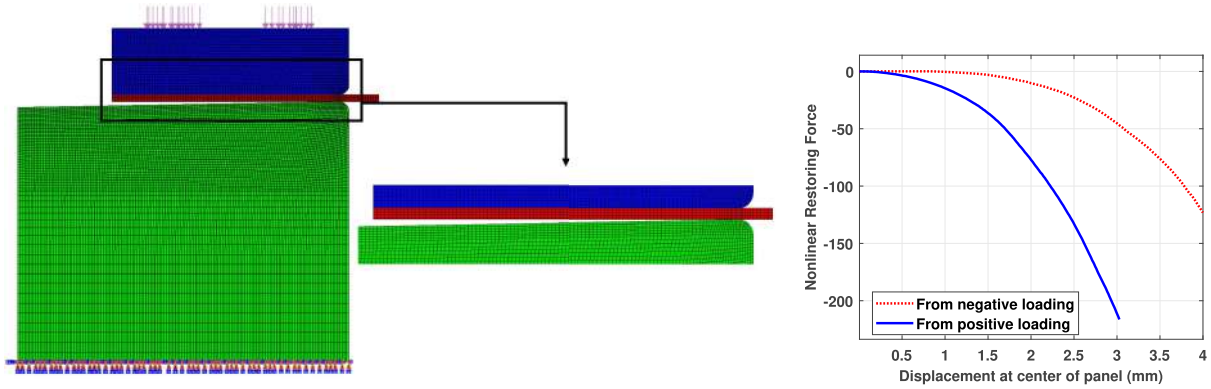

Figure 4: (left) BYU-UW 2D FE model [38]; (right) difference modal force-displacement curve associated with friction.

*3.3. NMA of ROM identified using QSMA (*BYU-UW*)*

The BYU-UW team consisted of the co-authors M.S. Allen, D. Shetty and C. Payne. The BYU-UW team used the finest contact mesh by far, as preliminary results suggested that this was needed to obtain accurate damping predictions at the amplitudes of interest (for the selected contact model specified below). In combination with the limited time and resources, however, the system had to be simplified to a 2D model (Fig. 4-left), assuming unit thickness in the z-direction. As a result, the cantilever nature of the support (pillars) had to be neglected. The effect of the latter simplification on the natural frequencies was found to be less than 1 % [37]. Four-node plane strain elements (i.e. CPE4 elements in ABAQUS) were used to mesh all the parts; higher order elements seemed to produce unreasonable contact pressure (i. e. scalloping in the pressure). The maximum panel mesh size was set to 0.5 mm over the contact length. The mesh was gradually made coarser further away from the contact regions, with a maximum length of 2 mm at the panel center. Five elements were used through the thickness of the panel.

Contact was modeled as hard in the normal direction, with the penalty method used to enforce this (to reduce convergence problems). Coulomb dry friction was used to simulate the tangential contact behavior with a friction coefficient of 0.6. The Lagrange multiplier method was used to impose constraints in the tangential direction. The bolt preload was simulated by applying a pressure along a line whose length is

equal to the washer diameter. The pressure level was taken to be an average of the total pressure acting along the z-direction, i. e. an average of the preload acting on the area covered by the three washers and zero pressure acting over the rest of the area. The estimated bolt tension force led to a pressure of 20.68 MPa applied over the length of 12 mm (washer diameter).
A single-degree-of-freedom (modal) model was used as a ROM, which contains a polynomial element in the modal coordinate in series with an Iwan element [50]. Effectively, this is a combination of the modal (parallel-series) Iwan model [51, 52], which captures the frictional nonlinearity, and a single degree-of-freedom implicit condensation and expansion ROM [53] to capture geometric nonlinearity. The parameters of the nonlinear elements (polynomial and Iwan model) were identified using QSMA [48]. First, a quasi-static analysis was carried out where interfacial slip was constrained (by setting the contact to 'Rough' in ABAQUS). The polynomial coefficients describing the geometric nonlinearity were then obtained by a regression of the modal force-displacement curve. Based on a convergence study, the polynomial was truncated to fifth order, where terms of order higher than three were used in order to capture static modal coupling to some extent. Then, a second quasi-static analysis was carried out with frictional sliding allowed. The resulting modal force-displacement curves look very similar to that shown in Fig. 3-left and are not depicted for brevity. The difference of the two modal force-displacement curves (interface locked vs. slipping) is attributed to friction only. Consequently, the parameters of the modal Iwan element were identified from that difference curve [38]. This step relies on Masing's rules for constructing the full hysteresis loop from the initial loading curve. However, as discussed in Subsect. 3.2, Masing's rules do not apply in the present case. In order to proceed, one ROM was identified for the two difference curves separately, the one obtained for positive and for negative loading (Fig. 4-right) and the subsequent analysis was applied to both models.
The shooting method in conjunction with arc-length continuation was applied to the ROM to compute the periodic modal oscillation as function of amplitude (Nonlinear Normal Mode) [54]. This way, the amplitude-dependent modal frequency was obtained. Compared to estimating the modal frequency from the QSMA directly, the effect of higher harmonics can be considered to some extent. However, the frictional nonlinearity was not considered in this step. To account for the frictional softening, the modal frequency ω was corrected as

$$\omega(a) = \sqrt{(\omega_{\mathrm{gnl}}(a))^2 + \Delta k_{\mathrm{fric}}(a)}\,, \tag{1}$$

where a is the modal amplitude, ω_{gnl} is the modal frequency obtained as described above (considering geometric nonlinearity only), and Δk_{fric} is the change of modal stiffness due to friction. Δk_{fric} was obtained as the secant of the frictional hysteresis curve, constructed using Masing's hypothesis from the modal Iwan element [55, 56]. Similar to the FAU approach, the modal damping ratio was determined as $D = \Delta W/(4\pi E_{\mathrm{p}}^{\mathrm{max}})$, where ΔW is the dissipated energy per cycle, and it was used that $E_{\mathrm{p}}^{\mathrm{max}} = \omega^2 a^2/2$. As the geometric nonlinearity does not contribute to the dissipation, ΔW was simply obtained by calculating the area enclosed in the frictional hysteresis cycle.
The described approach seeks to address both nonlinear stiffness and damping effects, but it neglects coupling between the two. This assumption was explored in [38] and found to hold for a class of systems that seems to be relevant for the given benchmark system. One of the main limitations of the proposed ROM technique is that it assumes symmetric behavior, as it relies on Masing's rules. While this speeds up computations by allowing one to compute the initial loading curve instead of complete hysteresis cycles for each amplitude, it adds uncertainty to the frequency and damping predictions. Also, while the proposed method is applicable to 3D finite element models, the accuracy of the present effort was limited due to the simplifications inherent in the 2D model that was used.

3.4. Ring down simulation of ROM identified using QSMA, no geometric nonlinearity (NWPU)

The NWPU team consisted of the co-authors C. Xu and H. Yang. The NWPU approach has in common with the BYU-UW one that the parameters of the ROM were identified form a high-fidelity quasi-static FE analysis, and an Iwan model was used to describe the frictional behavior. In contrast to the BYU-UW approach, the ROM does not represent a single modal oscillator but was obtained by applying the Hurty-/Craig-Bampton method. The ROM only contains the panel and the panel was modeled as flat in its unstressed configuration. Here, the holes in the panel were neglected in order to obtain a regular mesh

with reasonable density. To justify this simplification, it was checked that the error made by neglecting the holes is less than 5 % with regard to the panel's ten lowest-frequency modes. The mesh was built in ABAQUS and is depicted in Fig. 5-left, where only the symmetric half is shown for brevity (symmetry was not exploited in the modeling); it contains 32 x 10 quadrilateral elements (S4R). The Hurty-/Craig-Bampton method was applied, where the boundary nodes are those indicated in red (Fig. 5-left). The static constraint modes corresponding to all boundary degrees of freedom were retained, along with ten fixed-interface normal modes. The boundary nodes on either side were rigidly connected to one virtual node each [48, 57, 58]. Each virtual node initially had six rigid-body degrees of freedom. The rotations were constrained, an Iwan element was applied to each translational degree of freedom in the tangential plane, and a linear spring was attached to the translational degree of freedom in the normal direction.
To identify the parameters of the Iwan (joint) elements, a high-fidelity quasi-static analysis was carried out in ABAQUS using the FE model shown in Fig. 5-middle. The model is composed of $72,256$ hexahedral elements with linear shape functions (C3D8). Conforming meshes were used at the contact interfaces panel-blade and panel-support. The bolt loading was modeled by defining a pretension section in ABAQUS, where the bolt is cut and a distributed pressure is applied to both sides. Three different friction coefficients (0.2, 0.4, 0.6) were considered; the final results correspond to a value of 0.4, where the experimental data base in [59] was used for orientation. The results did not deviate much within the given range of friction coefficients. Otherwise default settings were used for the contact solver. Tangential force-displacement curves in the x- and z-direction were obtained using quasi-static analysis. Results are shown for the x-direction in Fig. 5-right. A modified Iwan model [60] was used, which has four parameters: normal preload, friction coefficient, tangential contact stiffness and macroslip stiffness ratio. The initial slope in Fig. 5-right was used as tangential contact stiffness and the final slope was used as macroslip stiffness.
A half-sine force pulse with a maximum of 5 kN and a duration of 0.2 s was applied and the response was simulated using time step integration. The Hilbert-Huang transform [61] was applied to identify the amplitude-dependent frequency and damping.
Besides neglecting geometric nonlinearity, the simplification of the contact displacement field to rigid-body translations (as required for the virtual node treatment) can be viewed as an important limitation.

*3.5. Frequency Response Analysis of ROM, no geometric nonlinearity (*ICL*)*

The ICL team consisted of the co-authors C. Schwingshackl, M. Lasen, D. Dini, and L. Salles. The FE model used by the ICL is depicted in Fig. 6. It consists of the panel, the blades, the bolts and a section of the pillars. The rear interface of the pillar section was assumed to be tied to the ground. The solid mesh contains hexahedral elements with quadratic shape functions (C3D20). Two regions were refined, namely the concentric region around the bolts (to better capture the pressure cone developed from the bolt load), and the contact region between the rounded edges of the blades and the panel.

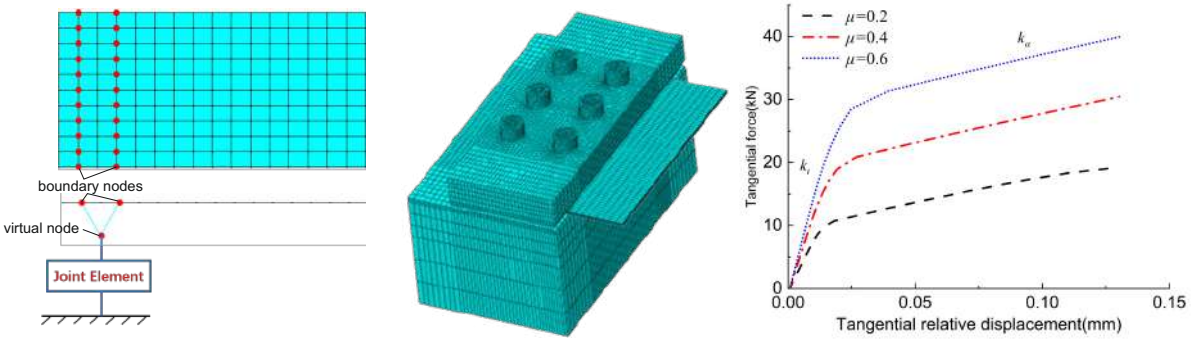

Figure 5: (left) Simplified NWPU FE model for ROM construction indicating boundary nodes, virtual-node model and joint element; (middle) high-fidelity FE model and (right) initial frictional loading curve used for identification of the joint element.

To simulate the bolting of the initially flat and unstressed panel, a static FE analysis was carried out using ABAQUS. The ABAQUS Bolt Load tool [62] was used to impose a load at the mid-plane of the cylindrical segment of the bolt lying between the blade and the pillar. The bolt load was applied in two steps, first at 0.1 % of the total load to activate the contact and then to full load. Coulomb dry friction was modeled, and the tangential contact was resolved using a penalty formulation, while hard contact was assumed to model the unilateral contact in the normal direction.

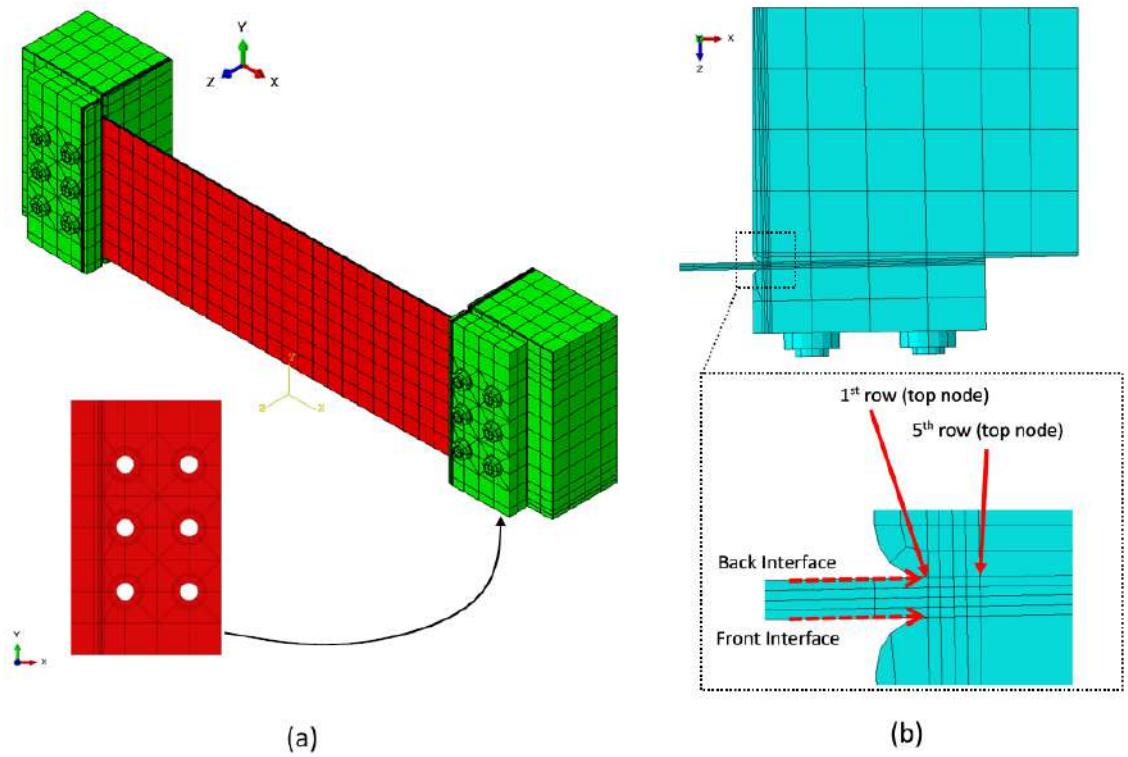

Figure 6: ICL FE mesh: (a) Overview (b) refinement in contact region.

Harmonic Balance was applied to compute the periodic steady-state frequency response for different excitation levels using the in-house tool FORSE [63, 64]. Here, the problem was restricted to the panel only. Nonlinear contact was modeled using 3D Jenkins elements, applied only to the vertex nodes of the underlying brick elements. It was assumed that only the contact region near the edge (Fig. 6(b)) contributes significantly to the frictional dissipation and the softening. Thus, the remaining region was assumed to be stuck and modeled as linear. A mesh convergence study was carried out for the active contact region, where additional element rows were successively included (Fig. 6(b)). After five rows, the frequency responses did not change significantly anymore and the results were considered as converged. Each element row contains nine vertex nodes, leading to a total of 180 contact nodes for the two sides of the panel and the two supports. Friction coefficient and tangential contact stiffness were selected in accordance with measurements obtained from the ICL 1D friction rig (see e. g. [59, 65, 66]) for a similar material pairing. The initial preload condition was adopted from the static FE analysis.
The fundamental and the third harmonic were retained in the Harmonic Balance analysis. The algebraic equation system was reduced to the nonlinear part, and the associated dynamic compliance matrix was set up using the mode shapes and natural frequencies from the FE modal analysis. A static correction was considered, which accounts for the residual compliance with respect to loads applied at the contact nodes. Instead of a base excitation, a concentrated load in the z-direction was applied to the center of the panel's rear side, and the response was measured in the same direction at the center of the panel's front side. The focus was placed on the frequency range of 15 Hz around the lowest linear natural frequency. A linear modal

fitting tool was applied to estimate the equivalent modal frequency and damping for each amplitude level [67].
The ICL team identified three limitations of their prediction approach: First, the geometric nonlinearity was neglected. Second, wear, surface tolerances and the surface finishing were not considered, and it is believed that these aspects are an important driver of variability expected in experiments. Finally, no contact parameters were available for the given type of joint and material pairing, so that values had to be adopted for a different yet similar contact.

*3.6. NMA of ROM (*USTUTT*)*

The USTUTT team consisted of the co-authors M. Krack, J. Gross and P. Hippold. The model included the panel, the blades and the complete support structure (pillars and rear plate). USTUTT and ETH were the only institutions that exploited the symmetry of the system by reducing the problem domain to only a half section (Fig. 7). Accordingly, the x-displacement of the symmetry plane was constrained. The bolts and washers connecting the rear plate to the slip table were not modeled. Instead, the nodes associated with the bore holes were constrained. The 3D CAD geometry was meshed using solid finite elements. A relatively fine, regular mesh of hexahedral elements with quadratic shape functions was used to model the free part of the panel ($58 \times 4 \times 40$ C3D20 elements in x, y, z direction, respectively). The two nominal contact interfaces (pillar-panel; panel-blade) were meshed by quadrilateral elements (panel) and triangular elements (pillar and blade) with linear shape functions. The 900 vertex nodes on each panel side were used as integration points within a node-to-surface contact formulation, treating the panel nodes as dependent ones. The remaining solid sections were rather coarsely meshed. This led to a total number of about 45,000 solid elements.
The bolts and washers used to mount the panel were also modeled using solid elements. The bolt preload was distributed uniformly at the bolt ends, and as concentrated force in the middle of the blind hole in the support structure. The preload simulation was carried out using a static FE analysis step where both contact and geometric nonlinearity were considered.
To reduce the model order, a nonlinear substructuring method was developed that is able to account for both contact and geometric nonlinearity [40]. The geometric nonlinearity was modeled in a non-intrusive way using implicit condensation [68, 69]. The computational effort for this essentially increases cubically with the number of retained component modes. It is common practice to apply component mode synthesis on system level and retain the relative displacements at the contact nodes. In conjunction with a fine contact mesh, the described modeling of contact and geometric nonlinearity (using implicit condensation) would lead to prohibitive computational effort. To overcome this, the system was split into free part of the panel and remaining system (Fig. 7). This permits to apply an appropriate reduction to the interface and restrict the implicit condensation to the free part of the panel. Further, conventional component mode synthesis can be applied to reduce the model order of the remaining system, and a fine contact mesh can be used because the associated component modes are irrelevant for the implicit condensation. More specifically, the free part of the panel was reduced to the three lowest-frequency bending-type fixed-interface normal modes and three interface modes (rigid-body translations in x- and y-directions and rotation about z-axis); i. e., six generalized coordinates are used in the reduced component model of the thin-walled region. The other rigid-body-type interface modes were constrained due to the difficulties described below, and also no elastic interface modes were retained. The remaining system, shown in gray in Fig. 7, was reduced to the static constraint modes associated with the aforementioned three interface modes as well as the relative displacements at the 900 contact nodes on each side of the panel, and the 30 lowest-frequency fixed-interface normal modes (all modes up to 18.9 kHz). The preloaded configuration was used as reference for the creation of the reduced model of the remaining system.
The implicit condensation of the free part of the panel is associated with two important difficulties: First, the preloaded configuration should be used as reference for the creation of the reduced model (as for the remaining system). Second, the substructure has rigid body modes. To account for the preloaded configuration, the interface displacements obtained in the static preload simulation were stored and imposed in a separate static analysis of the panel substructure. Subsequently, the reaction forces at the interface were stored, and the constraints were removed to derive the tangent stiffness and mass matrices of the free structure. Then,

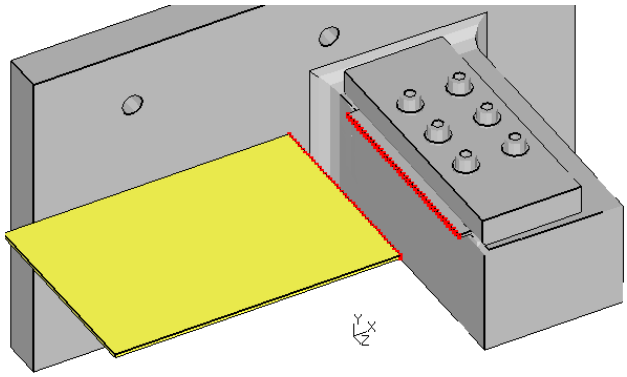

Figure 7: USTUTT approach to divide the assembly into thin-walled region (yellow) and support region (gray). Red nodes indicate the substructure interface.

the static load cases for the implicit condensation were set up as linear combinations of the component modes (retained fixed-interface normal modes and interface modes), multiplied from the left by the tangent stiffness matrix. Here, the load scale factors were set in such a way that the maximum displacement of the linearized system equals the panel thickness. Only the axial interface mode was scaled down by a factor of 1,000 in order to prevent buckling. To deal with the second difficulty (the rigid body modes), inertia relief was activated in the width (z-) direction, while the interface was constrained to prohibit rigid body motion in the thickness (y-) direction. Note that the x-displacement was constrained by the aforementioned symmetry condition. For the y-direction, inertia relief resulted in numerical difficulties, so that it was decided to exclude the associated interface mode from the implicit condensation modeling, but to retain that mode in the linear reduction basis. This way, geometric nonlinearity associated with the corresponding rigid body motion is neglected, which appears reasonable. The coefficients of the quadratic and cubic polynomials in the coordinates of the component modes were obtained by a conventional least-squares fit [40].
The contact was modeled assuming a time-constant normal preload (adopted from the static analysis) with a friction coefficient of 0.5. To this end, the relative motion in the contact normal direction was rigidly constrained. The Bouc-Wen model was used to account for some micro-slip behavior, and it was parameterized according to the experimentally identified model obtained for a similar material pairing and temperature in [66]. The same contact parameters were used throughout the interface (regardless of the local pressure). The number of about 900 contact elements on either side of the panel is rather high for the intended Harmonic Balance analysis. Thus, the subset of active (not permanently sticking) contacts was estimated, and the remaining (sticking) contacts were modeled as linear-elastic with the selected contact stiffness. To estimate the active set, all contacts were modeled as sticking and a static load was applied by imposing the lowest-frequency mode shape with an amplitude so that the maximum bending deformation equals the panel thickness. A contact was considered active if the corresponding tangential contact force exceeded 50% of the respective slip limit. This permitted a reduction of the active contact coordinates by a factor of about two.
A nonlinear modal analysis according to the Extended Periodic Motion Concept [70] was carried out using Harmonic Balance with a truncation order of 1. The nonlinear terms were evaluated using the alternating frequency-time scheme with 256 time samples per period.
The research group identified two main limitations of the pursued prediction approach: First, because of the current lack of an own experimental database, the parametrization of the contact law was a rather wild guess (friction coefficient; stiffness-pressure dependence neglected). Second, a time-constant normal load was assumed.

3.7. Frequency Response Analysis of ROM (ETH)

The ETH team consisted of the co-authors A. A. Morsy and P. Tiso. As in the case of the USTUTT approach, the problem was reduced to a symmetric half and according contraints were applied. The model

included the half panel and the blade, while the pillar was assumed as rigid, so that only its surface geometry had to be considered (Fig. 8). The 3D CAD geometry was meshed using ABAQUS with solid hexahedral elements with quadratic shape functions (3,000 C3D20 elements); the mesh is shown in Fig. 8. The mesh of the free part of the half panel (Component 1) was discretized using $16 \times 2 \times 20$ elements in x, y, z direction, respectively.

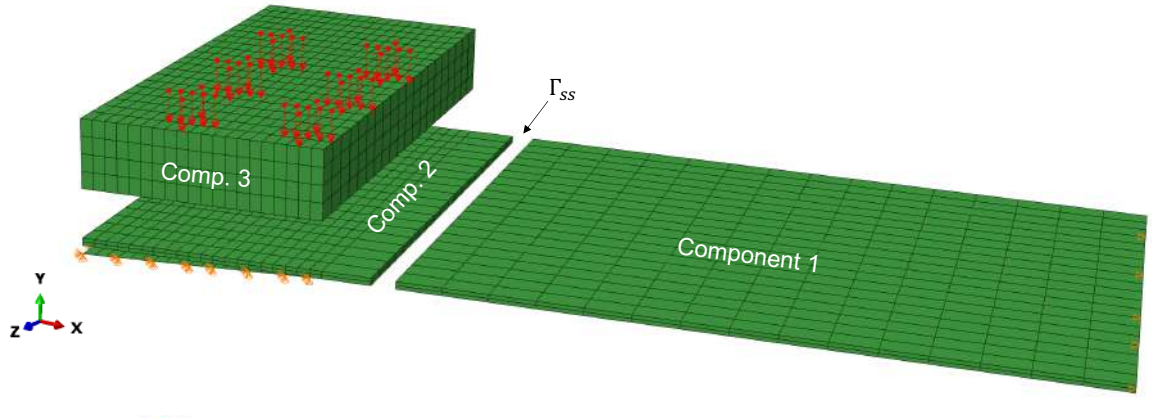

Figure 8: Illustration of ETH FE model, boundary conditions and substructuring approach. Nodes at which the bolt loads were applied are highlighted in red. Γ_{ss} is the interface connecting Components 1 and 2.

The bolts, bolt holes and washers were not modeled. The bolt preload was instead distributed uniformly to the seven vertex nodes near each bolt location as indicated in Fig. 8. The preload simulation of the initially flat and unstressed panel via the bolts was done analogous to the USTUTT approach, taking into account the geometric nonlinearity within the free part of the panel and the frictional contact at the two interfaces (panel-blade; panel-pillar). The contact model is described further below.
The dynamic substructuring strategy was similar to the USTUTT one, as the panel was split into a free and a clamped part (Component 1 and 2, respectively), and that geometric nonlinearity was only considered in the free part. Also, the preloaded configuration was used as reference for the creation of the reduced model. A fixed-interface Component Mode Synthesis approach was applied to the free part of the panel. The internal dynamics was reduced to the three lowest-frequency fixed-interface normal modes and the associated six Static Modal Derivatives (SMDs). An SMD $\frac{\partial \boldsymbol{\phi}_i}{\partial \eta_j}$ describes the change of mode shape $\boldsymbol{\phi}_i$ with respect to the modal coordinate η_j. The SMDs were computed by taking the derivative of the eigenvalue problem governing the mode shapes, where the sensitivity of the inertia terms was neglected, see e. g. [71]. The interface separating Components 1 and 2 was also reduced. To this end, an eigenvalue problem was set for the nodal degrees of freedom at the interface by constraining the internal nodes in the unassembled configuration (see e.g. [72]). Again, the three lowest-frequency normal modes and the associated six SMDs were retained. This led to a total of 18 component modes for the free part of the panel, which made it computationally feasible to model the geometric nonlinearity in the reduced space. The reduced stiffness tensors were computed intrusively [73] using YetAnotherFEcode [74]. Components 2 and 3 were reduced using the (static) Guyan method. More specifically, Component 2 was reduced to the static constraint modes associated with the generalized coordinates at the interface (Γ_{ss}) and the nodal coordinates at the two contact interfaces; Component 3 was reduced to the static constraint modes associated with the nodal coordinates at the contact interface and those coordinates to which the bolt load was applied. With the described Component Mode Synthesis, the total number of DoFs was reduced from 48,777 to 4,209.
The contact was modeled using 3D Jenkins elements, applied to the 21×21 grid of vertex nodes on each side of the panel, leading to a total of 882 elements. Since the group has no corresponding experimental database, the contact parameters were selected based on the available literature. A hyper reduction was applied to the contact model, relying on an Augmented Jacobian Projection method in conjunction with Energy Conserving Sampling and Weighting, with parameters (tolerances, amplifications) set similar to

[41]. Here, the reduction was carried out in the frequency domain, and no further kinematic restriction was introduced to the contact interface. The reduction was carried out once for the whole amplitude range and results in a reduced number of 154 Jenkins elements (instead of 882) based on which the contact forces were computed in the reduced model.
The periodic steady-state frequency response to harmonic base excitation was computed using Harmonic Balance with a truncation order of 3, in conjunction with arc-length continuation using the tool NLvib [75]. The nonlinear terms were evaluated using the alternating frequency-time scheme with 1024 samples per period for the contact forces. Only 13 samples per period were used for the geometrically nonlinear terms, which is sufficient to avoid aliasing errors for cubic-order polynomials with a harmonic order of 3 [76]. Material damping was modeled as Rayleigh Damping by setting the modal damping ratio equal to 0.3 % for the system's two lowest-frequency modes (first bending and first torsion mode). The base excitation was modeled as inertia loading, $\boldsymbol{f}_{\mathrm{ext}}(t) = A\boldsymbol{M}\boldsymbol{b}\cos(\Omega t)$, where A determines the magnitude of the imposed acceleration, $\boldsymbol{M}$ is the mass matrix, $\boldsymbol{b}$ is a Boolean vector with non-zero entries only for degrees of freedom in the y-direction, Ω is the angular excitation frequency, and t denotes time. The frequency response curves were computed for different acceleration levels A. The angular excitation frequency of the resonance peak was taken as amplitude-dependent natural angular frequency ω. The modal damping ratio D was computed according to single-nonlinear-mode theory [77],

$$\mathrm{D} = \frac{\|\hat{\boldsymbol{q}}_1^{\mathrm{H}}\hat{\boldsymbol{f}}_{\mathrm{ext},1}\|}{2\hat{\boldsymbol{q}}_1^{\mathrm{H}}\boldsymbol{M}\hat{\boldsymbol{q}}_1\omega^2}, \tag{2}$$

where $\|\square\|$ denotes the Euclidean norm, $\hat{\boldsymbol{q}}_1$ is the vector of complex fundamental Fourier coefficients of the generalized coordinates, $\square^{\mathrm{H}}$ denotes the complex conjugate transpose, and the fundamental Fourier coefficient of the excitation forces is $\hat{\boldsymbol{f}}_{\mathrm{ext},1} = A\boldsymbol{M}\boldsymbol{b}$.
As in the USTUTT approach, the lack of an experimental database limits the predictive capacity with regard to the parameters of the contact law. Another source of inaccuracy could be present due to the way in which the bold loads were applied. Since bolt holes were not modelled, this could affect the overall contact distribution and therefore influence the effective stiffness of the frictional clamping.

3.8. Frequency Response Analysis of reduced beam model, no geometric nonlinearity (SU)

The SU team consisted of the co-authors H. Jalali, N. Jamia, J. Taghipour, H. Haddad Khodaparast, and M.I. Friswell. The SU approach stands out in the sense that the system was simplified to a one-dimensional model, namely a beam with imperfect boundary conditions. The panel (beam) was considered as initially arched, assuming a half-sinusoidal shape with a maximum deflection of 2 mm at the center. The beam was discretized using 50 offset straight Euler-Bernoulli elements with three degrees of freedom per node [78]. Here, the offset distance for different elements alongside the beam length is considered equal to the pre-deflection corresponding to the element mid-point. It should be remarked that the initially submitted results were obtained for a flat beam and led to a much lower natural frequency than that expected from a 3D FE analysis. Subsequently, the model was revised to account for the described initially arched geometry, leading to a natural frequency much closer to that of the 3D FE model. Geometric (bending-stretching) nonlinearity was assumed to be small and therefore neglected, although it seems feasible to extend the proposed modeling approach accordingly (e. g. von-Karman beam theory). A schematic of the beam model is shown in Fig. 9.
The finite stiffness of the support was modeled via linear springs acting in the transversal direction (k_w) and in the rotational direction (k_θ), and via a nonlinear frictional element accounting for micro-slip behavior in the axial direction. The axial boundary force, P_{b} in this nonlinear element is governed by the differential law,

$$\dot{P}_{\mathrm{b}} = \left[k_{x1} + \frac{\dot{u}_{\mathrm{b}}}{|\dot{u}_{\mathrm{b}}|}(k_{x2}\,u_{\mathrm{b}} - \lambda P)\right]\dot{u}_{\mathrm{b}}\,, \tag{3}$$

where u_{b} is the axial displacement at the respective boundary. Eq. 3 can be interpreted as a modified Valanis model [79, 80]. Herein, k_{x1} is the stiffness of the linear spring in the axial direction, k_{x2} controls the slope

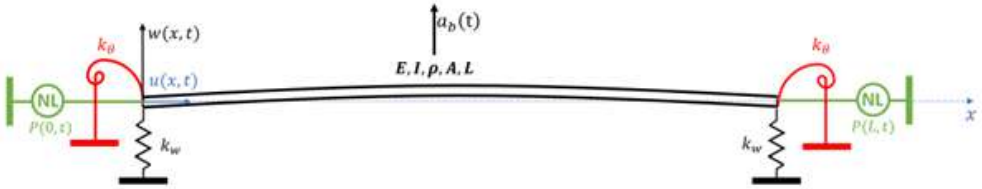

Figure 9: SU 1D curved beam model of the pre-deformed plate structure.

of the hysteresis loop in the macro-slip region and λ controls the transition from stick to macro-slip region. The parameter values were estimated from experience and are listed in Tab. 3.

Table 3: Parameter values estimated by SU for the modified Valanis model.

k_x [N/m]	k_w [N/m]	k_θ [Nm/rad]	k_{x1} [N/m]	k_{x2} [N/m]	λ
8×10^7	7.9×10^6	800	4×10^7	1×10^{13}	7×10^5

To facilitate the nonlinear analysis, the FE model was reduced to a single degree of freedom by truncating to the fundamental mode of the underlying linear system. The steady-state response to harmonic base excitation near the lowest-frequency bending mode was simulated using time step integration. The amplitude-dependent modal frequency and damping ratio were obtained from the amplitude resonance points obtained for different base excitation levels. A nonlinear modal fitting approach based on the Duffing equation was used to estimate natural frequency and damping ratio.
The described prediction approach has a few limitations. First, as it relies on beam theory, any variation of the system behavior (e. g. mode shape) in the third dimension (z-direction) is neglected. Second, geometric nonlinearity (bending-stretching coupling) was neglected. Third, the linear and nonlinear parameters of the clamping were based on experience.

3.9. Brief comparison of pursued approaches

It is useful to highlight some commonalities and differences among the prediction approaches. Only SNL and USTUTT included the rear plate into their model. FAU and ICL at least considered the cantilever nature of the support (pillars). Those aspects were neglected by the remaining groups due to their choice of the problem domain / boundary conditions. An overview of the FE meshing used for the free part of the panel is given in Tab. 4. Interestingly, only SU used beam elements and NWPU shell elements (but both neglected geometric nonlinearity), while the remaining groups used solid elements with 2 to 5 elements in the thickness direction, with a preference on hexahedral elements.

Table 4: Overview of FE models of the panel free part.

Research institution	element type	number of elements in $x-$, $y-$, z-direction	Young's modulus in GPa
BYU-UW	CPE4/CPE4R	$272 \times 5 \times 1$	200
FAU	C3D10	$(6,022)$	190
ETH	C3D20	$16 \times 2 \times 20$	195
ICL	C3D20	$24 \times 4 \times 8$	200
NWPU	S4R	$32 \times 1 \times 10$	200
SNL	HEX8 Selective Deviatoric	$504 \times 4 \times 100$	190
USTUTT	C3D20	$116 \times 4 \times 40$	206
SU	Offset beam	$50 \times 1 \times 1$	210

One difficulty that all groups had to face is to estimate the tensile force in the M6 bolts from the specified

tightening torque of 10.1 Nm. The selected values range from 6.1kN to 16.3kN, while most values are in a narrow range around 10kN (Tab. 5). This variability stems from the fact that only empirical formulae exist to determine how much torque is necessary to overcome the friction of the thread and that between nut and washer. The range of selected bolt tension forces is of a similar order of magnitude as the variability observed from instrumented bolts when tightening them with a torque wrench (see e. g. [81, 82, 23]). It should be noted that specifying the tightening torque is engineering standard and thus in line with the idea of the blind prediction challenge.
The number of contacts and the total contact area is an important difficulty which can generally lead to tremendous computational effort. This explains why only one group (SNL) modeled the contact between bolt head and washer, and the contact between washer and blade, whereas all remaining groups restricted the nonlinear contact analysis to the blade-panel and panel-support contacts. A number of different further strategies were employed to simplify the contact modeling:

- reduce the problem dimension from surface to line contact / 3D to 2D (BYU-UW)
- consider the normal contact as linear (SU; USTUTT; NWPU)
- reduce the active contact area by assuming certain parts as linear / sticking (ICL; USTUTT)
- reduce the relative displacement field to rigid-body translations (NWPU)
- pursue a hyper reduction to evaluate contact only at representative points (ETH)

An overview of key parameters of the contact models is given in Tab. 5. With the exception of SU, the contact is modeled using a finely resolved FE model by all groups (aiming for more predictive character). In the cases of BYU-UW and NWPU, this (high-fidelity) FE model was only used at an intermediate stage in order to identify a nonlinear (Iwan) element to be used within a ROM. The BYU-UW contact mesh is by far the finest, even though it is somewhat difficult to compare the considered line contact with the surface contacts used by the other groups. There is a tendency to model the contact as hard if the mesh is sufficiently fine, while FAU, ETH, ICL and USTUTT combine their coarser mesh with a finite contact stiffness (using Jenkins or Bouc-Wen elements, or the penalty method). It is remarkable that selected used friction coefficients span such a wide range from 0.15 to 0.67 (or even 0.8 in a sensitivity study), even though the key tribological parameters (material pairing, surface condition incl. roughness, preload and temperature) were specified. One possible explanation is the fact that the friction coefficients reported in the literature are almost entirely measured for sliding contacts (gross slip); it is not clear whether these are applicable to micro-slip situations where more or less the same patches of material slip and stick over and over again (partial slip).

Table 5: Overview of contact models applied on (high-fidelity) FE level; * assumes that the 21 nodes/cm of the line contact in the 2D model were accordingly extended in the third dimension. ** applies to active contact area, while a coarser mesh was used in the area presumed inactive. ∞ as contact stiffness means a hard contact model.

Research institution	mesh density [nodes/cm^2]	tang. contact stiffness [N/mm^3]	friction coefficient	bolt preload [kN]
BYU-UW	441*	∞	0.6	11.6
FAU	15.9	(slip dist. 1 μm)	0.15	10.0
ETH	8.82	$1 \cdot 10^5$	0.2	6.1
ICL	1.8**	$60 \cdot 10^3$	0.67	9.9
NWPU	56.7	∞	0.4	8.0
SNL	117.8	∞	0.5	9.8
USTUTT	17.2	$8 \cdot 10^3$	0.5	16.3

Interestingly, quite different analyses were carried out in order to determine the amplitude-dependent modal properties (Tab. 2). It is well known that both geometric and frictional contact nonlinearities can in many cases be treated as quasi-static, and this was exploited in the analyses of BYU-UW, FAU, and NWPU. Besides

QSMA, NMA was used (USTUTT; BYU-UW). ETH, ICL and SU analyzed the steady-state frequency response to harmonic near-resonant excitation, at different excitation levels, and extracted the natural frequency and damping ratio from the resonance peaks. Both NWPU and SNL analyzed the free decay / ring-down response and used time-frequency analysis (Hilbert-Huang transform and short-time fast Fourier transform, respectively) to determine instantaneous amplitude, frequency and amplitude decay rate. When applied to the same model, all approaches are expected to yield similar results provided that nonlinearity is weak and quasi-static, damping is light and modal interactions remain absent.

4. Experiment

To obtain a reference, the benchmark system was manufactured, assembled and tested in the course of the Tribomechadynamics Research Camp, August 8th - September 9th, 2022. The tests were mainly carried out by the co-authors A. Bhattu, S. Hermann, N. Jamia, under the supervision of M. Scheel, F. Müller, H. N. Özgüven, C. Schwingshackl and M. Krack. In the following, the instrumentation, the main test procedure, and important unexpected observations are briefly described. A more detailed description of the test sequence and the results of additional investigations (incl. cross-validation; disambiguation of different sources of uncertainty) are the content of a companion paper [83].

4.1. Test rig and measurement campaign

The test rig is illustrated in Fig. 10. As indicated in the definition of the challenge, the support structure is mounted on the slip table of a large shaker. First, the character of the base excitation was analyzed. More specifically, the symmetry of the excitation was checked by measuring the velocities of left and right blade at corresponding locations. A deviation of less than 2 % was obtained, which is deemed negligible. Consequently, the panel can in good approximation be viewed as being subjected to base excitation, and the panel response is defined relative to the base motion.

The contact pressure distribution may generally have an important effect on the effective stiffness and damping provided by a friction joint. A static pressure film was mounted between each interface between panel and pillar and between panel and blade, and removed before the dynamic tests. Fig. 11 shows an exemplary result. The contact area indicated by the pressure film was 34.1 cm^2. The color scale was taken from the manufacturer's specification for an average temperature of 26° C and relative humidity of 60%. Apparently, the pressure distribution was in good approximation uniform, with a pressure range of $12-19$ MPa, excluding small patches of high pressure near the bolt hole. The results for the contact between panel and pillar indicate white lines because of machining marks on the pillar. The pressure film results obtained for other tested configurations were indistinguishable from that shown in Fig. 11.

A rapid control prototyping system (dSPACE ControlDesk with a MicoLabBox) was used to run the feedback-controlled nonlinear vibration tests. For control purposes, the base velocity was measured using a laser Doppler vibrometer (LDV) pointed to the right blade and a differential LDV is used to measure the response velocity at the panel center (relative to the left blade). The velocity data used to analyze the system behavior was acquired by a Multi-Point Vibrometer (MPV). A set of 15 points positioned in a 5×3 grid on the surface of the panel was considered as shown in Fig. 10. Additional velocity measurements were performed on the right and on the left blade to obtain an average base velocity.

To isolate the lowest-frequency nonlinear mode, phase-resonance tests were carried out following the method proposed in [77]. Accordingly, base velocity and panel response were brought into phase resonance using a phase-locked loop with synchronous demodulation for phase detection. The desired phase lag between response and excitation signal was achieved using a proportional-integral controller, which adjusts the excitation frequency. A sinusoidal voltage signal of the given (time-variable) excitation frequency and a specified level was generated and fed to the amplifier of the shaker. Once phase resonance had been achieved, the steady-state time series was recorded. By step-wise in-/decreasing the gain of the voltage signal, the phase-resonance (backbone) curve was tracked.

From the acquired measurement data, the amplitude-dependent modal frequency and damping ratio, and the modal deflection shape (including higher harmonic content) can be identified. As shown in [77] using

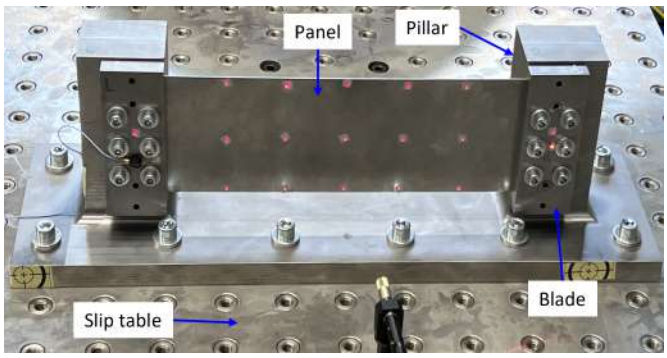

(a) Experimental benchmark system

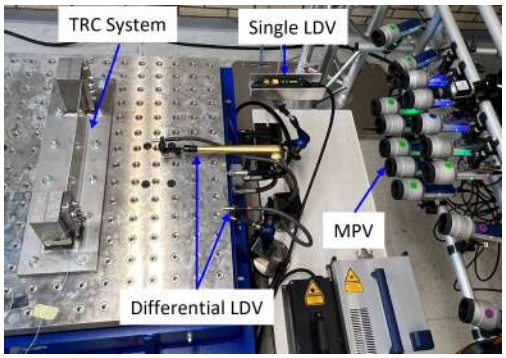

(b) Instrumentation

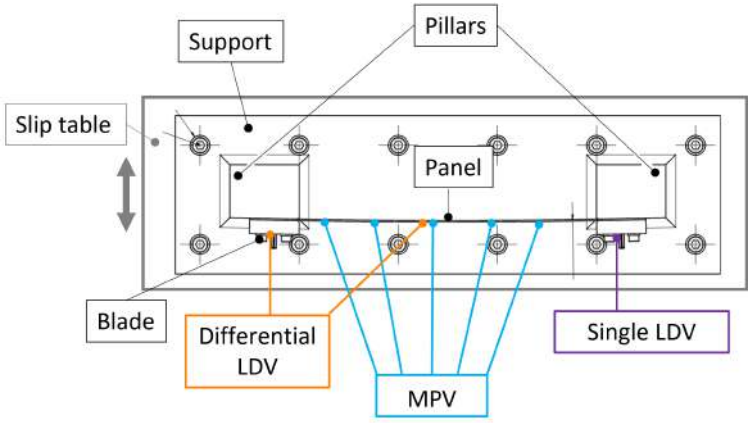

(c) Schematic top view

Figure 10: Experimental test rig used during the Tribomechadynamics Research Camp 2022.

single-nonlinear-mode theory, the phase resonant excitation frequency equals the modal frequency at a given amplitude. The modal damping ratio was obtained from the power balance of supplied and dissipated energy per oscillation cycle. A difficulty of base excitation is that the excitation forces cannot be directly measured to determine the supplied power. Instead, the power supplied by the imposed inertia forces was estimated using the model-free approach proposed in [77]. This requires response measurements at multiple locations to carry out a spatial integration. For the considered fundamental mode, the 5×3 grid was deemed sufficient[2].

For the purpose of serving as reference for the predictions, it is crucial to obtain experimental results of high confidence. Thus, several means were used to verify the amplitude-dependent modal properties obtained via the above described method. First, the consistency with the linear modal properties at low amplitudes was checked. To this end, a pseudo-random broadband signal was generated and fed to the shaker amplifier, and the frequency response function from base velocity to response velocity at the panel center (relative to the base) was estimated. The frequency band was wide enough to ensure a good estimation of the fundamental modal frequencies, and the excitation level was small enough to avoid the activation of significant nonlinearity. As the fundamental modal frequencies are well-separated, and the damping is moderate, the simple peak-picking method was deemed sufficient to identify natural frequencies and modal damping ratios. Second, the agreement with nonlinear results obtained with response-controlled tests [84] was verified. Third, the accuracy of the amplitude-dependent modal properties was validated by predicting frequency-

[2]More specifically, 5 points in the length direction yield an error $< 0.1\%$ for the value of the damping ratio in the case of a clamped-clamped beam. The 3 points in the width direction are expected to capture the potential three-dimensional character of the deflection shape.

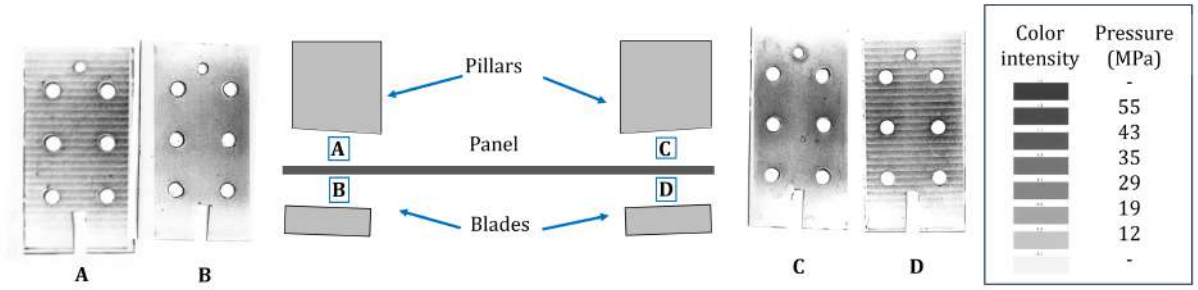

Figure 11: Exemplary pressure film results.

response curves for constant excitation level (using single-nonlinear-mode theory) and comparing the results with reference measurements. For brevity, the results of the latter two cross-validations are only shown in the companion paper [83]. Further, a number of direct repetitions were done, as well as repetitions with intermediate dis- and re-assembly. Finally, two nominally identical panels were manufactured and tested. Thanks to the symmetry, the panels can be mounted in two ways, leading to four tested configurations.

4.2. Important unexpected observations

Three unexpected observations were made during the measurement campaign:

1. The *thermal sensitivity* appears to have caused a considerably higher variability than the reassembly (even in the linear case).
2. There was a visible *panel curvature* in the unloaded configuration.
3. At higher amplitudes, indications of a 1 : 2 *modal interaction* between the first bending and the first torsion mode were found.

Concerning the *thermal sensitivity*, it should be mentioned that the tests were carried out in a laboratory without temperature control. Thus, the room temperature was well correlated with the outside temperature, which ranged between 23° C and 28° C depending on the day and time during the day. The panel temperature was generally different from the room temperature, due to the heat transfer from the shaker, and possibly also due to the panel heating up when it underwent high-level vibrations. It is plausible that a temperature change of the panel affects its prestress field, which influences its linear and nonlinear dynamic behavior. Consequently, a considerable variability was observed. In the following, we refer to the described variability (arguably) caused by thermal sensitivity as *time-variability*.
The photo in Fig. 12 shows the *panel curvature* when the panel is simply placed onto a (flat) ground. The flatness deviation is about 1.2 mm. As the curvature is very similar among the tested panels, the curved shape is attributed to the manufacturing process (rolling). The flatness deviation exceeds the general tolerance of 0.4 mm according to ISO 2768-mK specified in the original technical drawing. Due to time constraints, it was not possible to manufacture new panels that meet the specified flatness tolerance before the measurement campaign, and it can be argued that the specified tolerance is too tight for a sheet metal of the given dimensions and material formed by rolling. Thanks to the symmetry of the panel, it is possible to mount it both ways (initial panel curvature *aligned* or *misaligned* with pillars). Interestingly, this leads to a significant difference already for the linear natural frequency. When the curvature was aligned with the pillars, the linear natural frequency was at 103.0 Hz $\pm$ 1 %; when the panel was misaligned, it was at 107.5 Hz $\pm$ 1 %. It is plausible that the misalignment leads to a higher prestress in the mounted configuration and thus a higher stiffness and natural frequency. It was observed that the deviation from panel to panel was smaller than the time-variability and the *alignment-variability*. As mentioned before, the disambiguation of the different sources of variability is an important focus of the experimental companion paper [83]. The nonlinear tests were also carried out for both the aligned and the misaligned panel side.

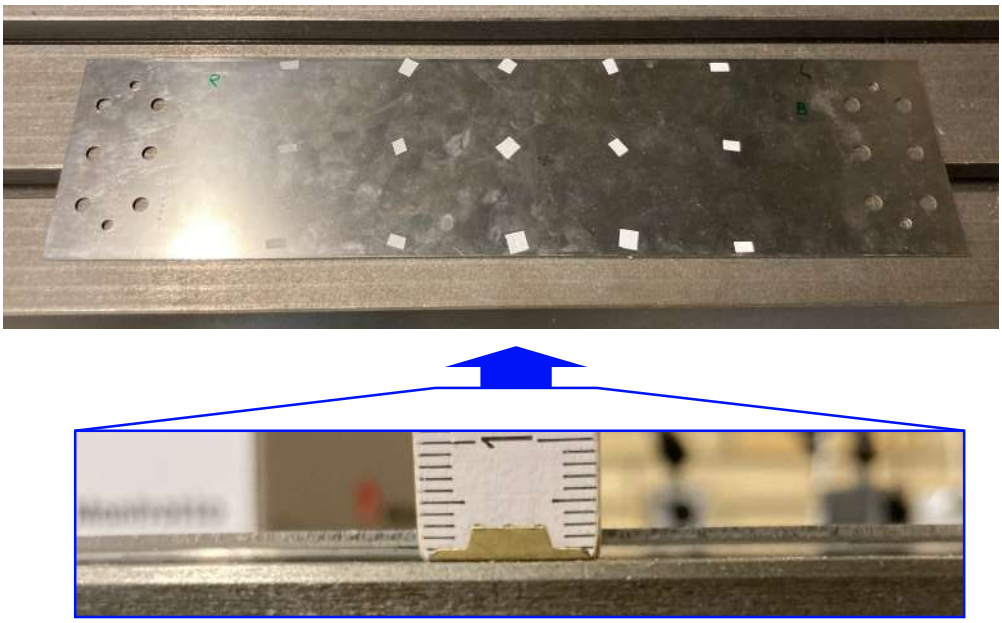

Figure 12: Photo of initial panel curvature.

The two lowest-frequency modes are the first bending and the first torsion mode, respectively. The experimentally identified mode shapes are depicted in Fig. 13-top. In the aligned configuration, the first torsion mode has a frequency of about 190 Hz, leading to a frequency ratio of about $1:1.9$. Further, the first torsion mode has a damping ratio of only $< 0.04\%$, which is about one order of magnitude less than that of the first bending mode. This condition is likely to amplify possible internal resonance phenomena. To determine whether or not a strong *modal interaction* takes place, the individual modal (m) and harmonic (h) contributions to the period-averaged mechanical energy $E(m,h)$ were estimated from the steady-state velocity data acquired during phase resonance testing. In the linear resonant case, the only non-negligible contribution should be $E(1,1)$. Fig. 13-bottom shows the contribution of the second harmonic of mode 1 and the second harmonic of mode 2, relative to $E(1,1)$. The remaining harmonic and modal contributions never exceeded 3% and are thus below the depicted range. In both, the aligned and the misaligned configuration, an appreciable second harmonic of the fundamental bending mode ($E(1,2)$) contributes to the response, which can be explained by the quadratic nonlinearity typical for initially curved plates. The contribution $E(1,2)$ increases almost monotonically and reaches a maximum of only about 10% energy fraction. In the aligned configuration, an internal resonance phenomenon is clearly observed: $E(2,2)$ reaches a peak at 45% energy fraction. In the misaligned configuration, in contrast, the contribution of the second mode is negligible. This is attributed to the fact that the frequency ratio is closer to 1:2 in the aligned configuration. More specifically, the frequency ratio is 1.89 in the aligned and 1.84 in the misaligned configuration. Assuming a perfectly symmetric plate subjected to an ideal base excitation, one would still expect that the torsion mode does not respond. However, the mounting of the panel on the pillars destroys the symmetry of the setup. The pillars undergo a slight cantilever-type deflection. As a result, the bending mode also exhibits larger deflections towards the upper edge of the panel (Fig. 13-top-left). Apparently, this is sufficient to permit the observed nonlinear interaction with the first torsion mode.

5. Results

In this section, we finally confront the core results of the predictions made by the different groups with each other and with the experimental reference. First, the results for the linear modal frequency are discussed, followed by the amplitude-dependent modal frequency and damping ratio.

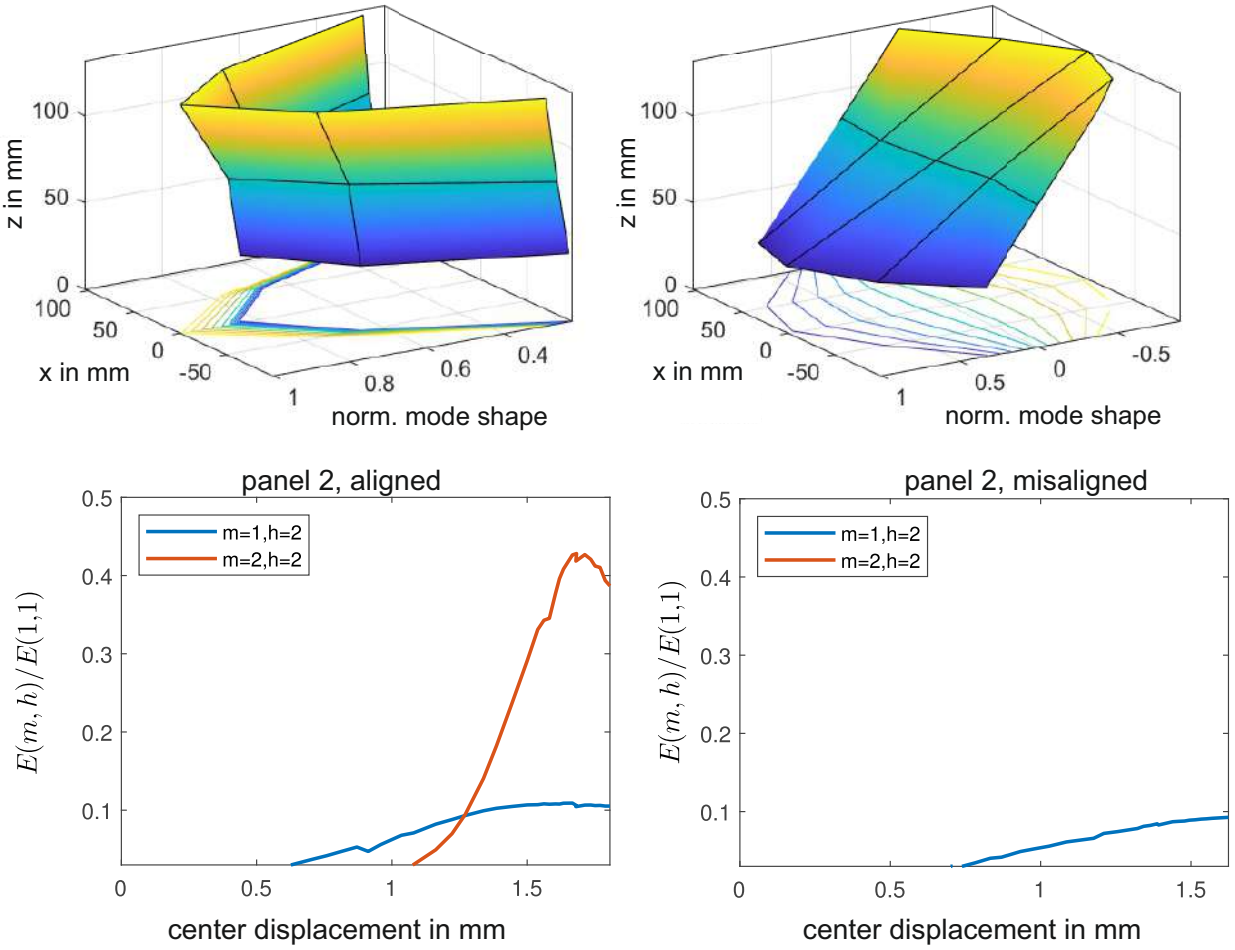

Figure 13: Illustration of modal interaction: low-amplitude mode shapes (top-left) first bending, (top-right) first torsion; (bottom) dominant modal and harmonic contributions to vibration energy in the aligned/misaligned configuration of panel 2.

5.1. Linear modal frequency

The results for the linear natural frequency of the lowest-frequency (bending) mode are shown in Fig. 14. Each acquired measurement result is regarded as an equally valid reference. Thus, the complete range of the experimental results acquired during the test campaign is shown throughout this section. As explained in Sect. 4, this range is due to reassembly-variability, time-variability (thermal sensitivity) and configuration-variability (mis-/alignment of initially curved panel with support), and the different sources of variability are analyzed individually in [83]. Most predictions are fairly close to the experimental results, albeit slightly higher. Indeed most predictions fall within the bounds obtained by SNL taking into account manufacturing tolerances (panel thickness), expected bounds of material properties (material density, Young's modulus) and contact state (tied vs. cutoff). The USTUTT prediction is a slight outlier at the upper end, which is attributed to multiple aspects: relatively high Young's modulus (cf. Tab. 4; e. g. 206 GPa vs. 190 GPa account for 4% alone); overly stiff representation of the contact, in particular, due to rigidly constraining relative motion in contact normal direction (constant normal load assumed for simplicity). The NWPU prediction is an outlier at the lower end, which may be because only the bolt hole was fixed for the linear natural frequency analysis, and because possible geometric hardening during assembly was neglected. Without the two outliers, the nominal predictions are all within a range of ±4 %.

It is concluded that the linear natural frequency can be predicted well, as long as no major simplification (too stiff/flexible coupling) is made. The SNL results suggest that the slight offset between predicted and ex-

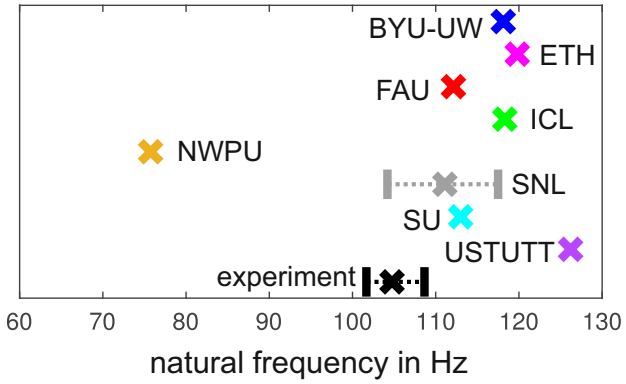

Figure 14: Linear natural frequency of lowest-frequency (bending) mode.

perimental mean value is due to the deviation between nominal and as-manufactured system (manufacturing tolerances; spread of material properties).

5.2. Amplitude-dependent modal frequency

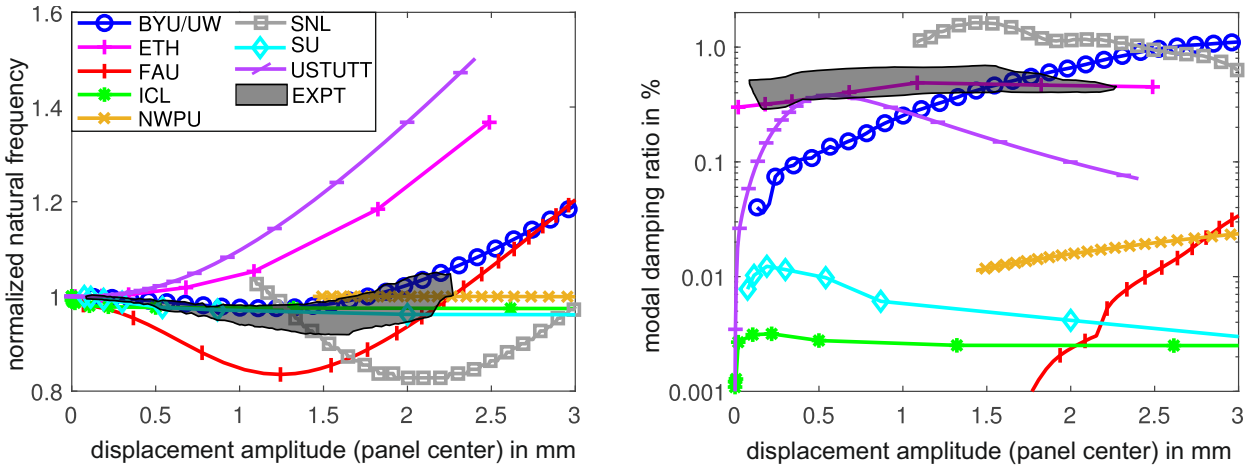

Figure 15: Amplitude-dependent modal properties: (left) modal frequency normalized by individual linear one; (right) modal damping ratio.

The amplitude-dependent modal properties are shown in Fig. 15. The modal frequency curves are normalized by the individual linear modal frequency presented in Fig. 14, to better show the relative variation with the amplitude. As amplitude measure, the transversal (y-)displacement at the panel's center is considered and $\sqrt{2}$ times the root mean square value is used. Note that this amplitude value equals half of the peak-to-peak amplitude if the signal is mono-harmonic, and, indeed, the latter amplitude measure was directly used in those predictions that a priori assume a mono-harmonic oscillation. On first sight, it seems that the variability spread of the experimental results increases with amplitude. However, this is an effect of the normalization: Since each experimentally obtained frequency-amplitude curves were normalized by their respective linear natural frequency, all curves start strictly at 1. The experimental results show a softening-hardening trend.

The predictions of the amplitude-dependent modal frequency show larger quantitative deviations than in the linear case, and even qualitative discrepancies appear. When geometric nonlinearity is neglected, only the monotonous softening due to the frictional nonlinearity is accounted for, which amounts to a modal

frequency shift of about −2 % (NWPU), −2.5 % (ICL) or −4 % (SU). The remaining groups accounted for geometric nonlinearity, and yet their predictions show substantial deviations.
For an initially arched beam/panel (with ideal boundary conditions), a pronounced softening-hardening effect would be expected, see e. g. [85]. This is in qualitative agreement with the FAU, SNL and BYU-UW predictions, and also with the experimental reference. In general, the extent of the frequency shift was over-predicted, and the predictions tend to be stiffer than the measurements, which is largely in line with the linear natural frequency results. This is mainly attributed to a too stiff representation of the contact. As the contact determines the boundary stiffness for the bending-stretching coupling, the contact has a crucial effect on the geometrically nonlinear behavior. More specifically, a coarse meshing and/or a stiff contact law leads to an over-prediction of the axial support stiffness, which, in turn, artificially increases the nonlinear bending-stretching coupling. This is demonstrated well by the FAU sensitivity analysis with regard to the contact stiffness parameter, see Appendix A. The above hypothesis also explains why the BYU-UW prediction, which relies on the by far finest mesh in the contact region, shows the smallest frequency shift caused by geometric nonlinearity. In contrast, FAU and SNL use a somewhat coarser contact mesh, and predict a much larger frequency shift (reaching about −17% in the softening regime). It is useful to recall that FAU assumed that the plate is stress-free in its arched and aligned configuration. It seems plausible that the missing prestress in this configuration leads to a more pronounced softening. Further, the softening predicted by USTUTT (frequency shift −0.05 %) is negligible and ETH only predicts hardening. In the USTUTT case, this is mainly attributed to an overly stiff representation of the contact, in particular, due to rigidly constraining the relative motion in contact normal direction. In the ETH case, this is attributed to an insufficient number of internal vibration modes retained during component mode synthesis, and to the overestimated contact stiffness (cf. Tab. 5). Those aspects may have led to a too stiff prediction by USTUTT and ETH.
Some inaccuracy is expected for the SNL and the BYU-UW approach due to the pursued dynamic analysis approach. Recall that the ring down results obtained by SNL look quite distinct from (slowly decaying) harmonic or periodic oscillations, and even contain a static offset (removed before determining the amplitude). Thus, the results may to some extent be contaminated by modal interaction. The analysis underlying the BYU-UW predictions a priori assumes that the vibration is dominated by a single harmonic and a single mode. This may explain the deviations to the experimental results at higher amplitudes, where pronounced contributions of the second harmonic and the second mode have been encountered.

5.3. Amplitude-dependent modal damping ratio

Concerning the amplitude-dependent (nonlinear) modal damping ratio, the results are very different among the individual groups (Fig. 15-right). A logarithmic scaling of the damping ratio had to be used in order to see (most of) the results in one plot. Most teams did not assume a linear damping. Thus,

Table 6: Linear damping selected by the research institutions.

Research institution	BYU-UW	FAU	ETH	ICL	NWPU	SNL	USTUTT	SU
linear damping	–	–	0.3%	–	–	0.5%	–	–

most predictions approach zero damping at asymptotically small amplitudes due to sticking friction. An exception is the ETH prediction, which postulates a linear damping ratio of 0.3 % (Tab. 6). Because the linear modal damping is predicted as zero by many teams, a normalization by a linear value is not possible in Fig. 15-right, in contrast to the modal frequency (Fig. 15-left). Interestingly, the experimentally identified damping ratio does not show any substantial decrease for small amplitudes. This is attributed to micro-slip, which is apparently under-predicted by most groups. ETH, ICL, USTUTT, SNL and SU predicted that the damping ratio initially increases, before it reaches a maximum and decreases slowly. This is in *qualitative agreement* with the experimental results. The remaining predictions do not show a decreasing damping ratio in the considered amplitude range, although most curves suggest a saturation at higher amplitudes. Recall also the large range of friction coefficients used by the different groups (Tab. 5). In the absence of

geometric nonlinearity and under constant normal load, an increased friction coefficient would lead to a stretching/shifting of the damping curve to higher amplitudes.
The order of magnitude of the predicted damping is strongly affected by the amount of predicted sliding friction in the contact interfaces, which, in turn, requires a sufficiently fine contact mesh and an appropriate description of the contact stiffness. As discussed before, a relatively coarse contact mesh was used by FAU, and the perhaps large elastic slip distance of 1μm prevents plastic slip to some extent, which may explain the under-prediction of the modal damping ratio. The quick increase of the damping may be a consequence of the relatively low friction coefficient, which results in large slip regions after onset of slip. Similarly, the virtual node treatment used by NWPU may have led to a too stiff interface representation and hence an under-prediction of the frictional damping. And assuming that the contact area is fully sticking except for a small region near the edge of the support may be an explanation for the under-prediction of the frictional damping by ICL. Further, neglecting the nonlinear bending-stretching coupling leads to an underestimation of the stretching, and thus smaller sliding distances and less energy dissipation [40], which affects the results obtained by ICL, NWPU and SU (cf. Tab. 2). At the other end, the modal damping ratio predicted by SNL is rather high; it exceeds 1% in a wide amplitude range and reaches a maximum of 1.6%. To some extent, this can be explained by the assumed linear damping ratio of 0.5 %. The numerical damping potentially associated with the time integration scheme (unknown for the given nonlinear problem setting), and the aforementioned contamination of the ring down signal may have led to an over-prediction of the damping ratio. In a certain amplitude range, the damping predictions of BYU-UW, ETH and USTUTT are in good *quantitative agreement* with the experimental reference. At higher amplitudes, however, BYU-UW and USTUTT over-/under-predict the damping, respectively. Here, it must be remarked that the BYU-UW results are subject to uncertainty, as the predictions rely on Masing rules, which were shown to be invalid, as discussed in detail in [38]. It should also be remarked that the experimental results may be contaminated at high amplitudes (> 1.2 mm), due to the encountered modal interaction, which invalidates the single-nonlinear-mode theory underlying the identification procedure. The ETH prediction matches the experimental results best, even in the low-amplitude range; however, this must be viewed in the light of the (empirically set) linear modal damping of 0.3 %.

5.4. Modal interaction

The experimentally observed 1:2 interaction between the fundamental bending and torsion modes did not receive a lot of attention in the predictions. As described above, SNL found indications of a modal interaction (pronounced higher harmonic content), although this was not further analyzed. The analysis of USTUTT was truncated to a single harmonic and also the model was truncated to the bending-type modes only, and was therefore unable to identify the aforementioned interaction. Similarly, the model of SU was truncated to a single mode. Moreover, quasi-static modal analyses are unable to capture modal interactions, which affects the predictions by BYU-UW and FAU. The BYU-UW team did decompose the quasi-static displacements into modal contributions, as was done in [86] and [87], to see if modal interactions were present but none were found; their model did not include torsion and so the interaction that ended up dominating was missed. The analysis pursued by ETH should generally be able to capture modal interactions. A possible explanation why no modal interaction was observed is the missing cantilever-type behavior of the support in their modeling (cf. Subsect. 4.2), and that that the $1:2$ internal resonance may require a softening nonlinearity, whereas ETH only predicted hardening. This is probably why ICL and NWPU did not detect any modal interaction either (geometric nonlinearity neglected).

6. Conclusions

In this work, the submissions to the Tribomechadynamics Research Challenge were presented and confronted with experimental reference. In view of the results, it can indeed be claimed that the benchmark system represents a true challenge for any prediction approach: First, both geometric (bending-stretching coupling) and frictional contact nonlinearity have a crucial influence on its vibration behavior. Second, its design provokes a mutual interaction between frictional dissipation and bending-stretching coupling (i. e.

an error in one part of the model is likely to yield an error in the other part as well). Third, the system's prestress is determined by an interplay of the bolted joints, the geometry imposed by the support, and the initial geometry of the panel. The initial geometry turned out not to be flat, in contrast to what every group assumed for their predictions, and it was found that this had a significant influence already on the linear natural frequency. Fourth, the doubly-clamped nature of the support makes the system sensitive to temperature changes, which also affects the prestress and leads to substantial time-variability. Finally, the first bending mode is close to a $1:2$ internal resonance condition with the first torsion mode, which was found to be responsible for the experimental evidence of a nonlinear modal interaction. In spite of these difficulties, experimental reference data of high confidence was obtained, where special attention was paid to cross-validate the results among different methods and capture the inherent variability.
Eight prediction approaches were pursued, ranging from 3D high-fidelity FE models to a reduced beam model, and also included interesting multi-fidelity strategies. Besides well-known approaches, rather recently developed model order reduction approaches were used, and in fact the complexity of the challenge triggered further method development. The linear natural frequency of the lowest-frequency mode was predicted quite accurately, where almost all predictions were within ± 4 % with a large overlap with the measurements. The results showed that for the doubly-clamped plate, the nonlinear bending-stretching coupling has a more important effect on the amplitude-dependence of the modal frequency than the frictional contact. The predictions overestimate the effect of bending-stretching coupling and tend to predict more hardening than softening, which is attributed to the overestimation of the axial support stiffness due to a too stiff contact model (too coarse mesh / too rigid contact law, not properly accounting for micro-slip). Most predictions of the amplitude-dependent modal damping ratio are in qualitative agreement with the experimental reference. The order of magnitude of the modal damping ratio was predicted well, as long as no over-simplification was made in the contact modeling (drastic reduction of active contact area; too stiff contact model). This applies, however, only to the intermediate amplitude range. At low amplitudes, the predictions underestimate the modal damping, which shows that further model improvement may be needed to correctly predict the micro-slip behavior.
A few recommendations for future work are derived from the TRChallenge:

- In view of the wide range of contact models and parameters (e. g. friction coefficient $0.15 - 0.8$), the establishment of a commonly available experimental database for well characterized material pairings, surface roughness properties and temperatures would be immensely valuable. Also, the community would benefit from further experiments elucidating whether the friction coefficients measured for macro-slip are valid in the micro-slip regime.
- Given that promising results on the prediction of micro-slip were obtained for extremely fine contact meshes, further effort towards reduced order modeling and multi-scale approaches seems necessary.
- Computationally feasible nonlinear prediction approaches should be developed that take into account the most relevant model uncertainties including contact parameters and surface topography, as-manufactured geometry of the solids and their prestress distribution.

To address the last point, a surrogate-based multi-fidelity approach and probabilistic inference could be suitable means. Such techniques were applied in [36] to the benchmark system.[3] By assuming reasonable parameter bounds on the support angle, the friction coefficient and the panel thickness, it is shown that one can generate samples of frequency-amplitude curves that span a range similar to the experimental data shown in Fig. 15-left.

Declaration of Competing Interest

The authors declare that they have no known competing financial interests or personal relationships that could have appeared to influence the work reported in this paper.

[3]The choice of low and high-fidelity models is critical in such an approach since one needs to make sure that all essential features of the solution (e. g. internal resonance) are also properly captured by the low-fidelity model. This approach, attempted in [36], therefore requires careful creation of models, as it does not rely on a proper model reduction technique.

Acknowledgements

M. Krack is grateful for the funding received by the Deutsche Forschungsgemeinschaft (DFG, German Research Foundation) [Project 450056469, 495957501].
This work presents results of the Tribomechadynamics Research Camp (TRC). The authors thank MTU Aero Engines AG for sponsoring the TRC 2022.
The authors are grateful to Maximilian W. Beck for aiding with the design of the benchmark system.
S. Hermann is grateful for the funding received by the EIPHI Graduate School, ANR-17-EURE-0002.
N. Jamia gratefully acknowledges the support of the Engineering and Physical Sciences Research Council through the award of the Programme Grant "Digital Twins for Improved Dynamic Design", grant number EP/R006768/1.
P. Tiso and A. A. Morsy acknowledge the funding of the Swiss National Science Foundation project "Meso-scale modeling of Friction in reduced non-linear interface Dynamics: MesoFriDy".
M.Y. Khan, J. Ortiz, D.A. Najera-Flores, R.J. Kuether, and P.R. Miles acknowledge that this article has been authored by an employee of National Technology & Engineering Solutions of Sandia, LLC under Contract No. DE-NA0003525 with the U.S. Department of Energy (DOE). The employee owns all right, title and interest in and to the article and is solely responsible for its contents. The United States Government retains and the publisher, by accepting the article for publication, acknowledges that the United States Government retains a non-exclusive, paid-up, irrevocable, world-wide license to publish or reproduce the published form of this article or allow others to do so, for United States Government purposes. The DOE will provide public access to these results of federally sponsored research in accordance with the DOE Public Access Plan https://www.energy.gov/downloads/doe-public-access-plan. This paper describes objective technical results and analysis. Any subjective views or opinions that might be expressed in the paper do not necessarily represent the views of the U.S. Department of Energy or the United States Government.

Appendix A. Sensitivity analysis of FAU

Some fuzziness was incorporated to the prediction of the amplitude-dependent natural frequency. The parameters of interest are chosen to be the elastic modulus E of the panel, the friction coefficient μ, and the absolute elastic slip distance γ. The results are depicted in Fig. A.1.

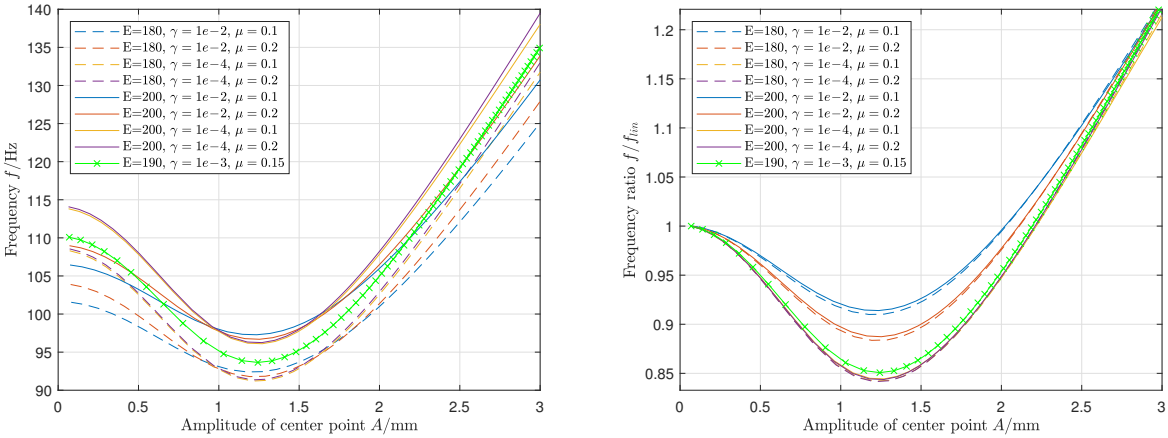

Figure A.1: Effects of uncertainties in material and contact parameters on the amplitude-dependent natural frequency of the first bending mode, analyzed by FAU: (left) non-normalized; (right) normalized; Unit of E is GPa, unit of γ is mm.

As one may expect, the natural frequency almost scales linearly with $\sqrt{E}$ so that the curves are almost indistinguishable for different values of E in the normalized plot. In contrast, the friction coefficient and the slip distance have an important influence on the effective axial support stiffness, and thus the extent of the natural frequency shift due to bending-stretching coupling.

References

[1] D. J. Segalman, L. A. Bergman, D. J. Ewins, Report on the SNL/NSF International Workshop on Joint Mechanics Arlington Virginia, 16-18 October 2006, Technical Report SAND2007-7761. Sandia National Laboratories, Albuquerque, NM, 2007.

[2] D. J. Segalman, L. A. Bergman, D. J. Ewins, Report on the SNL/AWE/NSF International Workshop on Joint Mechanics, Dartington, United Kingdom, 27-29 April 2009, Technical Report SAND2010-5458. Sandia National Laboratories, Albuquerque, NM, 2010.

[3] M. J. Starr, M. R. Brake, D. J. Segalman, L. A. Bergman, D. J. Ewins, Proceedings of the Third International Workshop on Jointed Structures, Technical Report SAND2013-6655. Sandia National Laboratories, Albuquerque, NM, 2013.

[4] M. R. W. Brake, D. J. Ewins, D. J. Segalman, L. A. Bergman, D. D. Quinn, Proceedings of the Fourth International Workshop on Jointed Structures, Technical Report SAND2016-9962. Sandia National Laboratories, Albuquerque, NM, 2016.

[5] A. T. Mathis, N. N. Balaji, R. J. Kuether, A. R. Brink, M. R. W. Brake, D. D. Quinn, A review of damping models for structures with mechanical joints, Applied Mechanics Reviews 72 (2020) 040802.

[6] B. J. Deaner, M. S. Allen, M. J. Starr, D. J. Segalman, H. Sumali, Application of viscous and iwan modal damping models to experimental measurements from bolted structures, ASME Journal of Vibration and Acoustics 137 (2015) 021012.

[7] D. R. Roettgen, M. S. Allen, Nonlinear characterization of a bolted, industrial structure using a modal framework, Mechanical Systems and Signal Processing 84 (2017) 152–170.

[8] S. Bograd, P. Reuß, A. Schmidt, L. Gaul, M. Mayer, Modeling the dynamics of mechanical joints, Mechanical Systems and Signal Processing 25 (2011) 2801–2826.

[9] E. P. Petrov, A high-accuracy model reduction for analysis of nonlinear vibrations in structures with contact interfaces, ASME Journal of Engineering for Gas Turbines and Power 133 (2011) 102503.

[10] S. Zucca, C. M. Firrone, M. M. Gola, Modeling underplatform dampers for turbine blades: A refined approach in the frequency domain, Journal of Vibration and Control 19 (2013) 1087–1102.

[11] N. N. Balaji, W. Chen, M. R. W. Brake, Traction-based multi-scale nonlinear dynamic modeling of bolted joints: Formulation, application, and trends in micro-scale interface evolution, Mechanical Systems and Signal Processing 139 (2020) 106615 (1–32).

[12] J. Armand, L. Pesaresi, L. Salles, C. Wong, C. W. Schwingshackl, A modelling approach for the nonlinear dynamics of assembled structures undergoing fretting wear, Proceedings of the Royal Society A 475 (2019) 20180731.

[13] A. R. Brink, R. J. Kuether, M. D. Fronk, B. L. Witt, B. L. Nation, Contact stress and linearized modal predictions of as-built preloaded assembly, ASME Journal of Vibration and Acoustics 142 (2020) 051106.

[14] N. N. Balaji, T. Dreher, M. Krack, M. R. W. Brake, Reduced order modeling for the dynamics of jointed structures through hyper-reduced interface representation, Mechanical Systems and Signal Processing 149 (2021) 107249.

[15] N. N. Balaji, M. R. W. Brake, The surrogate system hypothesis for joint mechanics, Mechanical Systems and Signal Processing 126 (2019) 42–64.

[16] R. M. Lacayo, L. Pesaresi, J. Groß, D. Fochler, J. Armand, L. Salles, C. Schwingshackl, M. S. Allen, M. R. W. Brake, Nonlinear modeling of structures with bolted joints: a comparison of two approaches based on a time-domain and frequency-domain solver, Mechanical Systems and Signal Processing 114 (2019) 413–438.

[17] J. H. Porter, N. N. Balaji, C. R. Little, M. R. W. Brake, A quantitative assessment of the model form error of friction models across different interface representations for jointed structures, Mechanical Systems and Signal Processing 163 (2022) 108163.

[18] M. R. W. Brake (Ed.), The Mechanics of Jointed Structures, Springer, 2017.

[19] M. R. W. Brake, M. Krack, C. W. Schwingshackl, Special issue: Tribomechadynamics, ASME Journal of Vibration and Acoustics 142 (2020) 050301.

[20] T. Dreher, M. R. W. Brake, B. Seeger, M. Krack, In situ, real-time measurements of contact pressure internal to jointed interfaces during dynamic excitation of an assembled structure, Mechanical Systems and Signal Processing 160 (2021) 107859.

[21] W. Chen, M. Jin, I. G. Lawal, M. R. W. Brake, H. Song, Measurement of slip and separation in jointed structures with non-flat interfaces, Mechanical Systems and Signal Processing 134 (2019) 106325 (1–22).

[22] M. Brons, T. A. Kasper, G. Chauda, S. W. B. Klaassen, C. W. Schwingshackl, M. R. W. Brake, Experimental investigation of local dynamics in bolted lap joints using digital image correlation, ASME Journal of Vibration and Acoustics 142 (2020) 051114.

[23] M. Ruan, The Variability of Strains in Bolts and the Effecton on Preload in Jointed Structures, Masters Dissertation, Rice University, Houston, TX., 2019.

[24] M. V. Karpov, Measurement of Bolt Dynamics in Jointed Structures Undergoing Dynamic Loading, Masters Dissertation, Rice University, Houston, TX., 2022.

[25] M. R. W. Brake, Contact modeling across scales: From materials to structural dynamics applications, Journal of Structural Dynamics 1 (2021) 49–135.

[26] J. H. Porter, M. R. Brake, Towards a predictive, physics-based friction model for the dynamics of jointed structures, Mechanical Systems and Signal Processing 192 (2023) 110210. doi:https://doi.org/10.1016/j.ymssp.2023.110210.
URL https://www.sciencedirect.com/science/article/pii/S0888327023001176

[27] M. H. Müser, W. B. Dapp, R. Bugnicourt, P. Sainsot, N. Lesaffre, T. A. Lubrecht, B. N. J. Persson, K. Harris, A. Bennet, K. Schulze, S. Rohde, P. Ijfu, W. G. Sawyer, T. Angelini, H. A. Esfahani, M. Kadkhodaei, S. Akbarzadeh, J.-J. Wu, G. Vorlaufer, A. Vernes, S. Solhjoo, A. I. Vakis, R. L. Jackson, Y. Xu, J. Streator, A. Rostami, D. Dini, S. Medina,

G. Carbone, F. Bottiglione, L. Afferrante, J. Monti, L. Pastewka, M. O. Robbins, J. A. Greenwood, Meeting the contact-mechanics challenge, Tribology Letters 65 (2017) 1–18.
[28] B. L. Boyce, S. L. B. Kramer, H. E. Fang, T. E. Cordova, M. K. Neilsen, K. Dion, A. K. Kaczmarowski, E. Karasz, L. Xue, A. J. Gross, A. Ghahremaninezhad, K. Ravi-Chandar, S.-P. Lin, S.-W. Chi, J. S. Chen, E. Yreux, M. Rüter, D. Qian, Z. Zhou, S. Bhamare, D. T. O'Connor, S. Tang, K. I. Elkhodary, J. Zhao, J. D. Hochhalter, A. R. Cerrone, A. R. Ingraffea, P. A. Wawrzynek, B. J. Carter, J. M. Emery, M. G. Veilleux, P. Yang, Y. Gan, X. Zhang, Z. Chen, E. Madenci, B. Kilic, T. Zhang, E. Fang, P. Liu, J. Lua, K. Nahshon, M. Miraglia, J. Cruce, R. DeFrese, E. T. Moyer, S. Brinckmann, L. Quinkert, K. Pack, M. Luo, T. Wierzbicki, The Sandia fracture challenge: Blind round robin predictions of ductile tearing, International Journal of Fracture 186 (2014) 5–68.
[29] B. L. Boyce, S. L. B. Kramer, T. R. Bosiljevac, E. Corona, J. A. Moore, K. Elkhodary, C. H. M. Simha, B. W. Williams, A. R. Cerrone, A. Nonn, J. D. Hochhalter, G. F. Bomarito, J. E. Warner, B. J. Carter, D. H. Warner, A. R. Ingraffea, T. Zhang, X. Fang, J. Lua, V. Chiaruttini, M. Mazière, S. Feld-Payet, V. A. Yastrebov, J. Besson, J.-L. Chaboche, J. Lian, Y. Di, B. Wu, D. Novokshanov, N. Vajragupta, P. Kucharczyk, V. Brinnel, B. Döbereiner, S. Münstermann, M. K. Neilsen, K. Dion, K. N. Karlson, J. W. Foulk III, A. A. Brown, M. G. Veilleux, J. L. Bignell, S. E. Sanborn, C. A. Jones, P. D. Mattie, K. Pack, T. Wierzbicki, S.-W. Chi, S.-P. Lin, A. Mahdavi, J. Predan, J. Zadravec, A. J. Gross, K. Ravi-Chandar, L. Xue, The second Sandia fracture challenge: Predictions of ductile failure under quasi-static and moderate-rate dynamic loading, International Journal of Fracture 198 (2016) 5–100.
[30] S. L. B. Kramer, A. Jones, A. Mostafa, B. Ravaji, T. Tancogne-Dejean, C. C. Roth, M. G. Bandpay, K. Pack, J. T. Foster, M. Behzadinasab, J. C. Sobotka, J. M. McFarland, J. Stein, A. D. Spear, P. Newell, M. W. Czabaj, B. Williams, H. Simha, M. Gesing, L. N. Gilkey, C. A. Jones, R. Dingreville, S. E. Sanborn, J. L. Bignell, A. R. Cerrone, V. Keim, A. Nonn, S. Cooreman, P. Thibaux, N. Ames, D. O. Connor, M. Parno, B. Davis, J. Tucker, B. Coudrillier, K. N. Karlson, J. T. Ostien, J. W. Foulk III, C. I. Hammetter, S. Grange, J. M. Emery, J. A. Brown, J. E. Bishop, K. L. Johnson, K. R. Ford, S. Brinckmann, M. K. Neilsen, J. Jackiewicz, K. Ravi-Chandar, T. Ivanoff, B. C. Salzbrenner, B. L. Boyce, The third Sandia fracture challenge: Predictions of ductile fracture in additively manufactured metal, International Journal of Fracture 218 (2019) 5–61.
[31] F. Müller, TRC Challenge - design documents, v1 Edition, DaRUS, 2022. doi:10.18419/darus-3147.
[32] M. R. W. Brake, C. W. Schwingshackl, P. Reuß, Observations of variability and repeatability in jointed structures, Mechanical Systems and Signal Processing 129 (2019) 282–307.
[33] S. I. Zare Estakhraji, M. Wall, J. Capito, M. S. Allen, A thorough comparison between measurements and predictions of the amplitude dependent natural frequencies and damping of a bolted structure, Journal of Sound and Vibration 544 (2023) 117397. doi:10.1016/j.jsv.2022.117397.
URL https://www.sciencedirect.com/science/article/pii/S0022460X22005806
[34] W. Lacarbonara, A theoretical and experimental investigation of nonlinear vibrations of buckled beams, Ph.D. thesis, Virginia Tech (1997).
[35] L. N. Virgin, Vibration of axially-loaded structures, Cambridge University Press, 2007.
[36] D. A. Najera-Flores, J. Ortiz, M. Khan, R. Kuether, P. Miles, A bayesian multi-fidelity neural network to predict nonlinear frequency backbone curves, Journal of Verification, Validation and Uncertainty Quantification (2024) 1–14doi:10.1115/1.4064776.
[37] D. Shetty, K. Park, C. Payne, M. Allen, Predicting nonlinearity in the tmd benchmark structure using qsma and sice, in: Nonlinear Structures & Systems, Volume 1, Springer, 2023, pp. 281–287.
[38] D. Shetty, M. S. Allen, K. Park, A new approach to model a system with both friction and geometric nonlinearity, Journal of Sound and Vibration (2023). doi:10.1016/j.jsv.2023.117631.
[39] M. Lasen, L. Salles, D. Dini, C. Schwingshackl, Tribomechadynamics challenge 2021: A multi-harmonic balance analysis from imperial college london, in: Nonlinear Structures & Systems, Volume 1, Springer, 2023, pp. 79–82.
[40] P. Hippold, F. Müller, J. Gross, M. Krack, Nonlinear dynamic substructuring of thin-walled jointed structures, in preparation (2024).
[41] A. A. Morsy, M. Kast, P. Tiso, A frequency-domain reduced order model for joints by hyper-reduction and model-driven sampling, Mechanical Systems and Signal Processing 185 (2023) 109744. doi:10.1016/j.ymssp.2022.109744.
URL https://www.sciencedirect.com/science/article/pii/S0888327022008135
[42] C. D. Team, Cubit 15.4 user documentation., Tech. Rep. SAND2019-3478 W, Sandia National Laboratories, Albuquerque, NM (2019).
[43] S. S. M. Team, Sierra/solidmechanics 5.10 user's guide., Tech. Rep. SAND2022-12223, Sandia National Laboratories, Albuquerque, NM (2022).
[44] S. S. D. D. Team, Sierra/sd - user's manual - 5.10., Tech. Rep. SAND2022-12518, Sandia National Laboratories, Albuquerque, NM (2022).
[45] R. J. Kuether, M. R. Brake, Instantaneous frequency and damping from transient ring-down data, in: Dynamics of Coupled Structures, Volume 4, Springer, 2016, pp. 253–263.
[46] M. Jin, M. R. W. Brake, H. Song, Comparison of nonlinear system identification methods for free decay measurements with application to jointed structures, Journal of Sound and Vibration 453 (2019) 268–293.
[47] M. Wall, M. S. Allen, R. J. Kuether, Observations of modal coupling due to bolted joints in an experimental benchmark structure, Mechanical Systems and Signal Processing (2022). doi:10.1016/j.ymssp.2021.107968.
URL https://doi.org/10.1016/j.ymssp.2021.107968
[48] R. M. Lacayo, M. S. Allen, Updating structural models containing nonlinear iwan joints using quasi-static modal analysis, Mechanical Systems and Signal Processing 118 (2019) 133–157. doi:https://doi.org/10.1016/j.ymssp.2018.08.034.
URL https://www.sciencedirect.com/science/article/pii/S0888327018305739

[49] E. E. Ungar, Loss factors of viscoelastic systems in terms of energy concepts, The Journal of the Acoustical Society of America 34 (7) (1962) 741. doi:10.1121/1.1937307.
[50] W. D. Iwan, A Distributed-Element Model for Hysteresis and Its Steady-State Dynamic Response, Journal of Applied Mechanics 33 (4) (1966) 893–900. doi:10.1115/1.3625199.
URL https://asmedigitalcollection.asme.org/appliedmechanics/article/33/4/893/385167/A-DistributedElement-Model-for-Hysteresis-and-Its
[51] D. J. Segalman, A Four-Parameter Iwan Model for Lap-Type Joints, Journal of Applied Mechanics 72 (5) (2005).
URL http://AppliedMechanics.asmedigitalcollection.asme.org/article.aspx?articleid=1415458
[52] D. J. Segalman, A Modal Approach to Modeling Spatially Distributed Vibration Energy Dissipation., Tech. Rep. SAND2010-4763, 993326, Sandia National Lab., Albuquerque, NM (2010).
[53] K. Park, M. S. Allen, Quasi-Static Modal Analysis for Reduced Order Modeling of Geometrically Nonlinear Structures, Journal of Sound and Vibration 502 (2021) 116076. doi:10.1016/j.jsv.2021.116076.
URL https://linkinghub.elsevier.com/retrieve/pii/S0022460X21001486
[54] M. Peeters, R. Viguié, G. Sérandour, G. Kerschen, J. C. Golinval, Nonlinear Normal Modes, Part II: Toward a Practical Computation Using Numerical Continuation Techniques, Mechanical Systems and Signal Processing 23 (1) (2009) 195–216. doi:10.1016/j.ymssp.2008.04.003.
URL https://www.sciencedirect.com/science/article/pii/S0888327008001027
[55] G. Masing, Self-stretching and hardening for brass, in: Proceedings of the 2nd International Congress for Applied Mechanics, Zurich, Switzerland, 1926, pp. 332–335.
[56] P. Jayakumar, Modeling and identification in structural dynamics, Report or Paper, California Institute of Technology, Pasadena, CA, issue: 87-01 Number: 87-01 Publisher: California Institute of Technology (May 1987).
URL https://resolver.caltech.edu/CaltechEERL:1987.EERL-87-01
[57] A. Singh, M. Wall, M. S. Allen, R. J. Kuether, Spider configurations for models with discrete iwan elements, in: Nonlinear Structures and Systems, Volume 1, Springer, 2020, pp. 25–38.
[58] E. Lindberg, N.-E. Hörlin, P. Göransson, Component mode synthesis using undeformed interface coupling modes to connect soft and stiff substructures, Shock and Vibration 20 (1) (2013) 157–170.
[59] C. Schwingshackl, E. Petrov, D. Ewins, Measured and estimated friction interface parameters in a nonlinear dynamic analysis, Mechanical Systems and Signal Processing 28 (2012) 574–584.
[60] D. Li, C. Xu, D. Wang, L. Wen, Numerical modeling and analysis of nonlinear dynamic response for a bolted joint beam considering interface frictional contact, in: ASME International Mechanical Engineering Congress and Exposition, Vol. 52033, American Society of Mechanical Engineers, 2018, p. V04AT06A053.
[61] N. E. Huang, Hilbert-Huang transform and its applications, Vol. 16, World Scientific, 2014.
[62] M. Smith, ABAQUS/Standard User's Manual, Version 6.9, Dassault Systèmes Simulia Corp, United States, 2009.
[63] L. Salles, L. Blanc, F. Thouverez, A. M. Gouskov, P. Jean, Dual time stepping algorithms with the high order harmonic balance method for contact interfaces with fretting-wear, Journal of Engineering for Gas Turbines and Power 134 (3) (dec 2011). doi:10.1115/1.4004236.
[64] E. P. Petrov, Explicit Finite Element Models of Friction Dampers in Forced Response Analysis of Bladed Disks, Journal of Engineering for Gas Turbines and Power 130 (2), 022502 (02 2008). doi:10.1115/1.2772633.
[65] L. Pesaresi, L. Salles, A. Jones, J. Green, C. Schwingshackl, Modelling the nonlinear behaviour of an underplatform damper test rig for turbine applications, Mechanical Systems and Signal Processing 85 (2017) 662–679. doi:https://doi.org/10.1016/j.ymssp.2016.09.007.
[66] A. Fantetti, L. R. Tamatam, M. Volvert, I. Lawal, L. Liu, L. Salles, M. Brake, C. W. Schwingshackl, D. Nowell, The impact of fretting wear on structural dynamics: Experiment and simulation, Tribology International 138 (2019) 111–124. doi:10.1016/j.triboint.2019.05.023.
URL http://www.sciencedirect.com/science/article/pii/S0301679X19302828
[67] D. J. Ewins, Modal testing: theory, practice and application, John Wiley & Sons, 2009.
[68] M. McEwan, J. Wright, J. Cooper, A. Leung, A finite element/modal technique for nonlinear plate and stiffened panel response prediction, in: 19th AIAA Applied Aerodynamics Conference, Fluid Dynamics and Co-located Conferences, American Institute of Aeronautics and Astronautics, 2001, p. 10pp. doi:10.2514/6.2001-1595.
[69] J. J. Hollkamp, R. W. Gordon, Reduced-order models for nonlinear response prediction: Implicit condensation and expansion, Journal of Sound and Vibration 318 (4–5) (2008) 1139–1153. doi:10.1016/j.jsv.2008.04.035.
[70] M. Krack, Nonlinear modal analysis of nonconservative systems: Extension of the periodic motion concept, Computers and Structures 154 (2015) 59–71. doi:10.1016/j.compstruc.2015.03.008.
[71] S. Jain, P. Tiso, J. B. Rutzmoser, D. J. Rixen, A quadratic manifold for model order reduction of nonlinear structural dynamics, Computers and Structures 188 (2017) 80–94. arXiv:1610.09902, doi:10.1016/j.compstruc.2017.04.005.
URL http://dx.doi.org/10.1016/j.compstruc.2017.04.005
[72] M. S. Allen, D. Rixen, M. Van Der Seijs, P. Tiso, T. Abrahamsson, R. L. Mayes, Substructuring in Engineering Dynamics: Emerging Numerical and Experimental Techniques, Springer, CISM International Centre for Mechanical Sciences, 2019.
URL https://doi.org/10.1007/978-3-030-25532-9
[73] J. Marconi, P. Tiso, D. E. Quadrelli, F. Braghin, A higher-order parametric nonlinear reduced-order model for imperfect structures using Neumann expansion, Nonlinear Dynamics 104 (4) (2021) 3039–3063. doi:10.1007/s11071-021-06496-y.
URL https://doi.org/10.1007/s11071-021-06496-y
[74] S. Jain, J. Marconi, P. Tiso, Yetanotherfecode. zenodo. (2020).
URL http://doi.org/10.5281/zenodo.4011281
[75] M. Krack, J. Gross, Harmonic Balance for Nonlinear Vibration Problems, Springer, 2019. doi:10.1007/

978-3-030-14023-6.
[76] L. Woiwode, N. N. Balaji, J. Kappauf, F. Tubita, L. Guillot, C. Vergez, B. Cochelin, A. Grolet, M. Krack, Comparison of two algorithms for harmonic balance and path continuation, Mechanical Systems and Signal Processing 136 (2020) 106503. doi:10.1016/j.ymssp.2019.106503.
[77] F. Müller, L. Woiwode, J. Gross, M. Scheel, M. Krack, Nonlinear damping quantification from phase-resonant tests under base excitation, Mechanical Systems and Signal Processing (2022). doi:10.1016/j.ymssp.2022.109170.
URL https://doi.org/10.1016/j.ymssp.2022.109170
[78] D. Hawla, H. Neishlos, Simulating curved beams via offset straight elements, Engineering Computations (1985).
[79] K. Valanis, A theory of viscoplasticity without a yield surface. part 1. general theory, Tech. rep., IOWA UNIV IOWA CITY DEPT OF MECHANICS AND HYDRAULICS (1970).
[80] K. C. Valanis, Fundamental consequences of a new intrinsic time measure. plasticity as a limit of the endochronic theory, Tech. rep., IOWA UNIV IOWA CITY (1978).
[81] S. A. Nassar, T. S. Sun, Surface roughness effect on the torque-tension relationship in threaded fasteners, Proceedings of the Institution of Mechanical Engineers, Part J: Journal of Engineering Tribology 221 (2) (2007) 95–103. doi:10.1243/13506501JET192.
URL https://doi.org/10.1243/13506501JET192
[82] Q. Zou, T. S. Sun, S. A. Nassar, G. C. Barber, A. K. Gumul, Effect of lubrication on friction and torque-tension relationship in threaded fasteners, Tribology Transactions 50 (1) (2007) 127–136. doi:10.1080/10402000601105490.
URL https://doi.org/10.1080/10402000601105490
[83] A. Bhattu, S. Hermann, N. Jamia, F. Müller, M. Scheel, H. N. Özgüven, C. W. Schwingshackl, M. Krack, Experimental analysis of the trc benchmark system, in review for Journal of Structural Dynamics (2024). doi:10.48550/arXiv.2403.07438.
[84] T. Karaağaçlı, H. N. Özgüven, Experimental modal analysis of nonlinear systems by using response-controlled stepped-sine testing, Mechanical Systems and Signal Processing 146 (2021) 107023. doi:10.1016/j.ymssp.2020.107023.
URL http://www.sciencedirect.com/science/article/pii/S088832702030409X
[85] G. Abeloos, F. Müller, E. Ferhatoglu, M. Scheel, C. Collette, G. Kerschen, M. R. W. Brake, P. Tiso, L. Renson, M. Krack, A consistency analysis of phase-locked-loop testing and control-based continuation for a geometrically nonlinear frictional system, Mechanical Systems and Signal Processing 170 (2022). doi:10.1016/j.ymssp.2022.108820.
[86] E. Jewell, M. S. Allen, I. Zare, M. Wall, Application of quasi-static modal analysis to a finite element model and experimental correlation, Journal of Sound and Vibration 479 (2020) 115376. doi:10.1016/j.jsv.2020.115376.
URL http://www.sciencedirect.com/science/article/pii/S0022460X20302078
[87] Singh, Aabhas, Allen, Matthew S., Kuether, Robert J., Multi-mode Quasi-static Excitation for Systems with Nonlinear Joints, Mechanical Systems and Signal Processing Vol. 185 (15 February) (2023) 109601.
URL https://doi.org/10.1016/j.ymssp.2022.109601